https://doi.org/10.5194/egusphere-2026-3713
Preprint. Discussion started: 15 July 2026

FRISO (v1.0): A physiological carbon flux model for simulating algal ^{13}C-fractionation

Yannick F. Bats[1], Appy Sluijs[1], Gert-Jan Reichart[1,2]

[1]Department of Earth Sciences, Faculty of Geosciences, Utrecht University, Princetonlaan 8, 3584 CB Utrecht, The Netherlands

[2]NIOZ Royal Netherlands Institute for Sea Research, 1797 SZ 't Horntje, The Netherlands

Correspondence to: Yannick F. Bats (y.f.bats@uu.nl)

Abstract. The CO_2-dependaency of stable carbon isotope fractionation (ε_p) during marine algal carbon acquisition is widely used as a proxy for past atmospheric pCO_2. However, a mechanistic model linking ε_p and pCO_2 that explains observations in the modern ocean, culture experiments and across Pleistocene glacial-interglacial cycles is still lacking. Here, we present a multi-compartment model of an algal cell that simulates environmental control on passive CO_2 diffusion, active HCO_3^- transport, and ^{13}C fractionation during C-fixation. Relative to previous models, our main new implementations include light-sensitive HCO_3^- acquisition and calcification, and daylength-dependent pyrenoid permeability, based on physiological expectations. The model is fitted to and tested with culture data of multiple dinoflagellate species and the coccolithophore *Gephyrocapsa huxleyi*. This shows robust performance across a wide range of parameter values from culture experiments, implying an appropriate representation of the mechanistic control of ^{13}C-fractionation in algal organic matter, potentially paving the way for sedimentary work.

1 Introduction

Reconstructions of the past partial pressure of carbon dioxide (pCO_2) in the atmosphere are essential for understanding and quantifying the relation between Earth's climate and global carbon cycling (IPCC, 2021). Beyond the reach of direct measurements on air bubbles enclosed in Antarctic ice (~1.5 Ma), proxies are applied. One important line of proxies is based on the CO_2-dependency of the preferential incorporation of ^{12}C over ^{13}C during carbon assimilation in marine phytoplankton relative to the surrounding dissolved CO_2 pool, termed ^{13}C-fractionation (Freeman & Hayes, 1992). Stable carbon isotope fractionation (ε_p) increases with higher dissolved CO_2 concentrations in most, if not all, algae (Bidigare et al., 1997; Brandenburg et al., 2022; Rost et al., 2002). Because ε_p and its CO_2-dependency are strongly type- and species-specific, taxon-specific approaches to describe and quantify the ε_p-CO_2 relationship are needed to accurately translate ε_p values into CO_2 reconstructions (Brandenburg et al., 2022). This might include biomarkers such as alkenones produced by specific coccolithophores, and dinoflagellate cysts (dinocysts) (e.g., Bidigare et al., 1997; Frieling et al., 2023; Hoins et al., 2015; Phelps et al., 2021).

https://doi.org/10.5194/egusphere-2026-3713
Preprint. Discussion started: 15 July 2026

Conventionally, the ε_p-CO_2 proxy is based on a diffusive model of ε_p (Farquhar et al., 1982; Francois et al., 1993), where CO_2 is assumed to passively diffuse into (and out of) the cell, where it is fixed by the enzyme rubilose-1,5-biphosphate carboxylase (Rubisco). Under higher CO_2 concentrations, more CO_2 passes through the cell, resulting in more ventilation (also referred to as leakage) of the internal inorganic carbon pool (Rost et al. 2002). This way, ^{13}C-fractionation during acquisition is closer to the maximally possible fractionation, which is determined by Rubisco. However, the simple diffusive model cannot explain culture and surface sediment alkenone-based ε_p values (Phelps et al., 2021) or ice core-based pCO_2 records over Pleistocene glacial cycles (Badger et al., 2019; Stoll et al., 2019). Clearly, it does not take the full complexity of algal ^{13}C-fractionation into account. Notably, in addition to CO_2, algae may use HCO_3^- as an inorganic carbon source (Burns & Beardall, 1987), which has a ~10 ‰ higher $\delta^{13}C$ than CO_2 (Mook et al., 1974). Along with Rubisco and leakage, this determines ε_p (Sharkey and Berry, 1985). In turn, environmental and physiological factors including growth rate, temperature, cell size, and shape, may impact leakage and HCO_3^- use (e.g., Cassar et al., 2006; Laws et al., 1997; Phelps et al., 2021; Popp, Laws, et al., 1998; Wilkes & Pearson, 2019).

Hitherto no mechanistic models exist that accurately simulate ε_p based solely on diffusion of CO_2, active uptake of HCO_3^-, and fixation by Rubisco. In addition, no model accurately simulates the effect of continuous light versus light/day cycles, and light intensity in general, on ε_p, without the need of other enzymes that induce additional isotope fractionation (Wilkes and Pearson, 2019), or *post hoc* parameterizations of "effective" fractionation (Holtz et al., 2017). Besides Wilkes and Pearson (2019) and Holtz et al. (2017), most multi-compartment flux-based approaches (Cassar et al., 2006; Holtz et al., 2015; Hopkinson, 2014; McClelland et al., 2017) do not explicitly incorporate light-dependent HCO_3^- transport. However, because HCO_3^- is a charged ion, its uptake requires active transport through the cell membrane and is therefore expected to depend on adenine triphosphate (ATP) produced during light-dependent photophosphorylation (Checchetto et al., 2012, 2013; Tester & Blatt, 1989). Indeed, light effects on ε_p have been recorded in coccolithophore culture experiments and alkenone surface sediment data (Phelps et al., 2021; Rost et al., 2002), and to a lesser extent in dinoflagellates (Hoins, Eberlein, Groβmann, et al., 2016).

In this study, we build upon the vast collection of modeling, culture and core-top studies that aim to constrain the mechanisms driving ε_p, to develop a four-compartment mechanistic model of ^{13}C-fractionation. The model simulates CO_2 diffusion, light-induced active uptake of HCO_3^-, and Rubisco-associated carbon fixation. We compare the newly developed model with published culture data on dinoflagellates, and the coccolithophore *Gephyrocapsa huxleyi,* and assess the various environmental parameters and physiological conditions that influence ^{13}C-fractionation. We show that this conceptually simple carbon uptake model, as first proposed by Sharkey and Berry (1985), accurately explains culture ε_p data.

2 Methods

2.1 The carbon flux and isotope fractionation model

The goal of our model – termed Fractionation of carbon isotopes In Simulated algal Organic matter (FRISO) – is to simulate ε_p values in bulk algal tissue. The formulation of ε_p is generally expressed as:

https://doi.org/10.5194/egusphere-2026-3713
Preprint. Discussion started: 15 July 2026

$$\varepsilon_p = \frac{\delta^{13}C_{CO_2} - \delta^{13}C_{algae}}{1 + \left(\frac{\delta^{13}C_{algae}}{1000}\right)} \quad (1)$$

This is algebraically derived from the fractionation factor alpha (α, Eq. 2), the delta notation of carbon isotopes ($\delta^{13}C$ in ‰, versus the Vienna Peedee Belemnite standard) and the epsilon formulation of isotopic fractionation (ε = [α – 1] x 1000).

$$\alpha = \frac{\left(\frac{^{13}C}{^{12}C}\right)_{CO2}}{\left(\frac{^{13}C}{^{12}C}\right)_{algae}} \quad (2)$$

This formulation of ε_p approaches the difference between $\delta^{13}C_{CO2}$ and $\delta^{13}C_{algae}$ ($\Delta\delta^{13}C_{CO2\text{-}algae}$).

To simulate ε_p, we devised a model in R (R Core Team, 2023) consisting of four compartments (cf., Hopkinson, 2014; Wilkes & Pearson, 2019), which represent the cytosol (*c*), chloroplast (*ch*), thylakoid (*t*) and pyrenoid (*p*) of an alga (Fig. 1). The fluxes and interactions of the DIC species CO_2 and HCO_3^- between and within these compartments are modeled using a system of ordinary differential equations (Eq. 7 - 22). Carbonate ion (CO_3^{2-}) fluxes are disregarded because of their negligible role in photosynthesis, and because CO_3^{2-} can implicitly be treated as part of the HCO_3^- pool due their relatively quick interconversion (Hopkinson, 2014; Zeebe & Wolf-Gladrow, 2001). The concentrations of CO_2 and HCO_3^- in the four compartments (*c*, *ch*, *t* and *p*) are referred to as *C* for CO_2, and *H* for HCO_3^- (e.g., *Cp*, *Hp*). CO_2 is fixed in the pyrenoid by Rubisco. All concentrations and rates of concentration changes within compartments are given in mol cm^{-3} and mol cm^{-3} s^{-1}, respectively. Carbonate chemistry within the model simulations is constrained using the *seacarb* package (Gattuso et al., 2023). For conversions from mol kg^{-1} to mol cm^{-3}, a water density of 1.025 kg L^{-1} is used. The model is fitted to culture data of dinoflagellates and *G. huxleyi* (Sect. 2.2.).

https://doi.org/10.5194/egusphere-2026-3713
Preprint. Discussion started: 15 July 2026

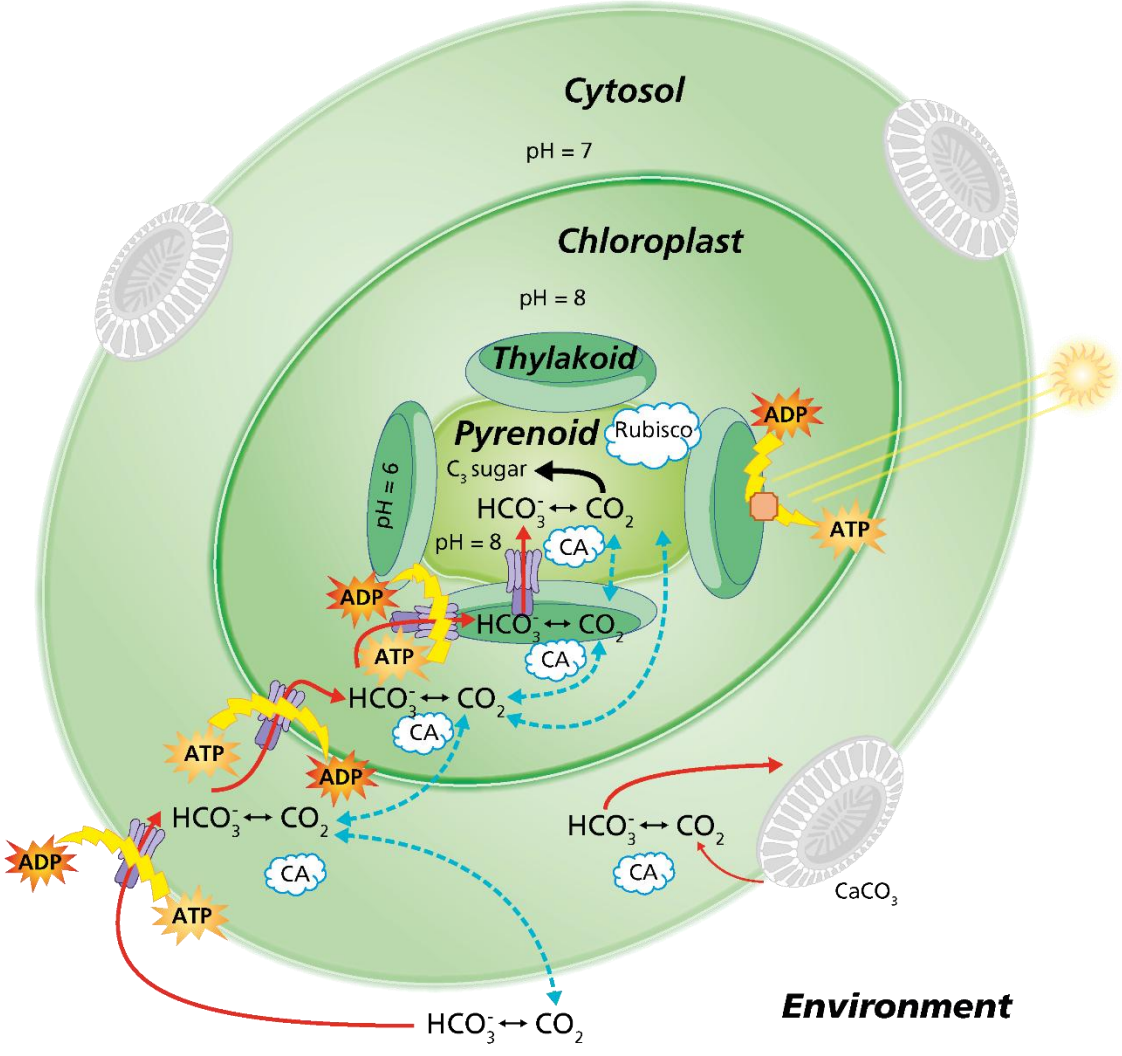

Figure 1: HCO_3^- and CO_2 fluxes in a conceptual four-compartment model (not to scale). HCO_3^- is actively taken up (red arrows) by membrane-bound transporters (purple channels) from the environment into the cytosol, from the cytosol into the chloroplast and from the chloroplast into the thylakoid. These membrane-bound transporters are driven by ATP, which is produced under the influence of light (photophosphorylation). CO_2 passively diffuses (blue dotted arrows) between the environment, cytosol, chloroplast, thylakoid and pyrenoid. Within the compartments, HCO_3^- and CO_2 are interconverted under the influence of carbonic anhydrase (CA). Within the pyrenoid, CO_2 is fixed by ribulose-1,5-bisphosphate carboxylase oxygenase (Rubisco). In calcifying algae, HCO_3^- is removed from the cytosol to form $CaCO_3$ and CO_2 is produced. The pH of each compartment is displayed, where the pH of the pyrenoid is assumed to be equal to that of the chloroplast.

2.1.1 Acquisition of CO_2 and HCO_3^-

CO_2 diffuses between the external environment (*e*) and the cytosol (*c*), between the cytosol and the chloroplast stroma (*ch*), between the chloroplast stroma and pyrenoid (*p*), and between the thylakoid lumen (*t*) and the pyrenoid (Fig. 1). The passive

https://doi.org/10.5194/egusphere-2026-3713
Preprint. Discussion started: 15 July 2026

transport of CO_2 between compartments (Eq. 1) depends on the concentration gradient ($C_x - C_y$), the compartment specific membrane permeability (p_m, in cm s^{-1}), the surface area (SA, in cm^2) of the membrane through which CO_2 diffuses, and the volume of the compartment (V, in cm^3) from or towards which CO_2 diffuses.

$$CO_2\,\text{transport}_{x\to y}\ (\text{mol cm}^{-3}\,\text{s}^{-1}) = \frac{SA_y}{V_y} p_m (C_x - C_y) \tag{3}$$

HCO_3^- is actively taken up (Eq. 2) from the seawater into the cytosol, out of the cytosol into the chloroplast, and from the chloroplast into the thylakoid, by membrane-bound transporter enzymes, with a rate following Michaelis-Menten kinetics. Considering HCO_3^- uptake occurs across the compartment membranes, the uptake rate is scaled to surface area and volumes of the respective compartments.

$$HCO_3^-\,\text{uptake}_{x\to y}\ (\text{mol cm}^{-3}\,\text{s}^{-1}) = \frac{u_{max}\cdot H_x}{K_n + H_x}\frac{SA_y}{V_x}$$
$$\text{where, } u_{max}\ (\text{mol cm}^{-2}\,\text{s}^{-1}) = u_b + f_{PFD}\cdot PFD \tag{4}$$

Here, K_n is the Michaelis (i.e., half-saturation) constant (in mol cm^{-3}), which likely varies between species (Rost, Riebesell, et al., 2006). We assume u_{max} to depend on light intensity (photon flux density, PFD) (Eq. 4), as light-induced ATP production (photophosphorylation) enhances membrane-bound transporter enzyme functioning (Sect. 2.1.2.) (Nakajima et al., 2013; Omata et al., 1999). For simplicity, we assume u_{max} to linearly depend on PFD, with factor f_{PFD} and base (no light) HCO_3^- uptake rate u_b. The unit of PFD is µmol photons m^{-2} s^{-1}, which is conventionally written as µE m^{-2} s^{-1}.

We add a simple calcification term ($calc$, in s^{-1}) in the HCO_3^- equation of the cytosol compartment (Eq. 6), which represents the rate at which HCO_3^- is removed from the cytosol for calcification. This calcification rate also depends on light/daylength (Grubb et al., 2024; Zhang & Gao, 2021) and is set to 0 for the non-calcifying dinoflagellates. Net calcification results in the removal of 0.85 units of HCO_3^- from the cytosol and the addition of 0.35 units of CO_2 to the cytosol (Middelburg, 2019).

2.1.2 Light-dependent C-acquisition

The influence of light intensity and daylength on ε_p observed in culture studies has been attributed to processes that concentrate inorganic carbon near Rubisco (e.g., Hoins, Eberlein, Groβmann, et al., 2016; Wilkes & Pearson, 2019). We include two generic light-dependent parameterizations. Firstly, we assume that the HCO_3^- uptake rate (u_{max}) depends on light intensity, i.e., photon flux density (PFD). Under the influence of light, excitation of the thylakoid membrane-bound photosystems results in ATP-production and pumping of protons (H^+) into the thylakoid lumen (photophosphorylation). Through an interplay of H^+ pumping and ATP-stimulated co-transport of ions such as Cl^-, Mg^{2+}, K^+ and HCO_3^-, cell compartments manage to control their pH and create a proton motive force necessary for, e.g., ATP production (Barber et al., 1974; Checchetto et al., 2012, 2013; Pottosin & Schönknecht, 1995; Tester & Blatt, 1989). Indeed, the rate of photophosphorylation in algae is closely linked to combined availability of light and HCO_3^- (Cohen & Jagendorf, 1974; Zolotareva et al., 2013). Moreover, the relative electron

https://doi.org/10.5194/egusphere-2026-3713
Preprint. Discussion started: 15 July 2026

transport rate in *G. huxleyi* is known to be forced by light (Grubb et al., 2024; Zhang & Gao, 2021). Resolving the biochemical complexity of the interactions between light and proton/ion exchange is beyond the scope of this model, so the light-dependent stimulation of HCO_3^- uptake is parameterized linearly (Eq. 4).

Secondly, in dinoflagellates specifically, concentration of Rubisco in pyrenoid structures tends to occur during the day around the cell center, whereas this disappears during the night, implying there is a diurnal forcing on pyrenoid configuration (Nassoury et al., 2001). In haptophytes (*Phaeocystis antarctica* specifically), pyrenoids become less condensed – and thus more diffuse – with light intensity (Moisan et al., 2006). To generically implement this in the model, we parameterized the pyrenoid permeability (p_p) as follows:

$$p_p = p_m \cdot f_{pd} \text{ where } f_{pd} \propto \text{daylength} \quad (5)$$

Where the pyrenoid membrane permeability factor (f_{pd}) scales normal membrane permeability (p_m), influenced by daylength with factor f_p.

2.1.3 Interconversion between HCO_3^- and CO_2

Within the four compartments, HCO_3^- and CO_2 are interconverted according to the acid dissociation constant (K_1) corresponding to the interconversion reaction $HCO_3^- + H^+ \leftrightarrow CO_2 + H_2O$. K_1 is constrained using the *seacarb* package in R (Gattuso et al., 2023; K_1 = 1.17x10^{-6} mol L^{-1}). The forward reaction rate (k_f) is represented by $\frac{10^{-\mathrm{pH}}}{\mathrm{K1}} \cdot 10^6$ and the reverse reaction rate (k_r) is represented by $\frac{\mathrm{K1}}{10^{-\mathrm{pH}}} \cdot 10^6$. The pH of the cytosol, chloroplast, thylakoid and pyrenoid are set to 7, 8, 6 and 8, respectively (cf. Wilkes & Pearson, 2019). We assume the interconversion between HCO_3^- and CO_2 to happen quasi-instantaneously because it is catalyzed by the enzyme carbonic anhydrase (CA), and therefore we multiply the reaction rates by a generic large number (10^6). The system is insensitive to the choice of this number, as long as it is not a limiting factor, and an order of magnitude bigger than 10^2. Consequently, smaller values result in reduced ε_p as the interconversion rate becomes a limiting factor.

2.1.4 Carbon fixation in the pyrenoid

Within the pyrenoid compartment, CO_2 (C_{ch}) is fixed into biomass under the influence of Rubisco with carbon fixation rate r_1. The fixation rate (r_1, in mol cm^{-3} s^{-1}) is constrained similarly to Wilkes and Pearson (2019), by multiplying average particulate organic carbon (POC, in mol) content with instantaneous growth rate (μ_i, in s^{-1}), scaled (i.e., divided) to cell volume (in cm^3), for cultured algal cells.

Here, μ_i is the instantaneous growth rate, which is the growth rate (μ) corrected for the duration of the photoperiod:

$$\mu_i = \frac{\mu \cdot (L+D)}{L - D \cdot resp} \quad (6)$$

https://doi.org/10.5194/egusphere-2026-3713
Preprint. Discussion started: 15 July 2026

Where, L and D are the length of the light and dark period, and *resp* represents dark respiratory carbon loss, which is assumed to be 15% (Rost et al., 2002; Laws and Bannister, 1980).

V_{ch} was based on V_{cell} (Table A1), which was approximated from POC (cf. Wilkes and Pearson, 2019) according to the equation from Menden-Deuer and Lessard (2000) for phototrophic dinoflagellates, and Popp et al. (1998) for *G. huxleyi*. Following Wilkes and Pearson (2019), the volumes and surface area of each compartment were then determined by assuming a spherical shape; $V_c = 0.847V_{cell}$, $V_{ch} = 0.09V_{cell}$,$V_t = 0.06V_{cell}$, and $V_p = 0.003V_{cell}$.

2.1.5 System of ODEs for carbon isotope dynamics

The abovementioned processes and parameterizations are incorporated into a system of ordinary differential equations (ODE) (Eq. 7-14) that simulate the inorganic carbon dynamics and carbon fixation. The model is run to steady state (i.e., the inorganic carbon fluxes are in equilibrium) using the *grind.R* R script for solving ODEs (De Boer, 2024).

$$\frac{dC_c}{dt} = k_{f1}H_c - k_{r1}C_c + \frac{SA_{cyt}}{V_{cyt}}p_c(C_e - C_c) - \frac{SA_{ch}}{V_{cyt}}p_{ch}(C_c - C_{ch}) + 0.35 \cdot calc \cdot H_c \quad (7)$$

$$\frac{dC_{ch}}{dt} = k_{f2}H_{ch} - k_{r2}C_{ch} + \frac{SA_{ch}}{V_{ch}}p_{ch}(C_c - C_{ch}) - \frac{SA_p}{V_{ch}}p_P(C_{ch} - C_p) \quad (8)$$

$$\frac{dH_c}{dt} = k_{r1}C_c - k_{f1}H_c - \frac{u_C H_c}{(K_n+H_c)}\frac{SA_{ch}}{V_{cyt}} + \frac{u_E H_e}{(K_n+H_e)}\frac{SA_{cyt}}{V_{cyt}} - 0.85 \cdot calc \cdot H_c \quad (9)$$

$$\frac{dH_{ch}}{dt} = k_{r2}C_{ch} - k_{f2}H_{ch} + \frac{u_C H_c}{(K_n+H_c)}\frac{SA_{ch}}{V_{ch}} - \frac{u_{CH} H_{ch}}{(K_n+H_{ch})}\frac{SA_t}{V_{ch}} \quad (10)$$

$$\frac{dC_t}{dt} = k_{f3}H_t - k_{r3}C_t - \frac{SA_p}{V_t}p_T(C_t - C_p) \quad (11)$$

$$\frac{dH_t}{dt} = k_{r3}C_t - k_{f3}H_t + \frac{u_{CH} H_{ch}}{(K_n + H_{ch})}\frac{SA_t}{V_t} \quad (12)$$

$$\frac{dC_p}{dt} = \frac{SA_p}{V_p}p_P(C_{ch} - C_p) + \frac{SA_p}{V_p}p_T(C_t - C_p) - r_1 + k_{f4}H_p - k_{r4}C_p \quad (13)$$

$$\frac{dH_p}{dt} = k_{r4}C_p - k_{f4}H_p \quad (14)$$

Using the steady state values of C_c, C_{ch}, C_t, C_p, H_c, H_{ch}, H_t and H_p, stable carbon isotope dynamics and fractionation terms are added to the system of ODEs (Eq. 15-22), with the assumption that the stable carbon isotope dynamics are in steady state. Included fractionation terms are associated with CA-mediated hydration of CO_2 to HCO_3^- (ε_{CH}), the CA-mediated dehydration of HCO_3^- to CO_2 (ε_{HC}), and the fractionation associated with Rubisco ($\varepsilon_{Rubisco}$), which is set to 24‰ for dinoflagellates (form II Rubisco) (Guy, 1993; McNevin et al., 2007; Robinson et al., 2003), and 11.1‰ for *G. huxleyi* (Boller et al., 2011). Although

https://doi.org/10.5194/egusphere-2026-3713
Preprint. Discussion started: 15 July 2026

the $\varepsilon_{Rubisco}$ value of *G. huxleyi* is relatively low, this has recently been confirmed by Wijker et al. (2026), who found a $\varepsilon_{Rubisco}$ value of ~13‰ for *G. oceanica*.

The $\varepsilon_{Rubisco}$ value for dinoflagellates falls within the range (19 – 24‰) found for the type II Rubisco associated with dinoflagellates (Guy, 1993; McNevin et al., 2007; Robinson et al., 2003). However, these values are based on the analysis of purified Rubisco from α-proteobacteria (*Rhodospirillum rubrum*) and γ-proteobacteria (endosymbiont of *Riftia pachyptila* tubeworms), with a relatively large range of values between and within these taxa. Therefore, it could be possible that dinoflagellate Rubisco fractionates with a different value. For example, the highest ε_p value found for cultured *A. tamarense* (~27‰) can only be reached if $\varepsilon_{Rubisco}$ is set to a higher value. The correct $\varepsilon_{Rubisco}$ value of dinoflagellate Rubisco fractionation remains uncertain and are important topics for future research.

Lastly, in the surrounding environment, we implement a temperature dependence of the kinetic carbon isotope fractionation associated with the CA-mediated interconversion of HCO_3^- and CO_2, similar to that of the non-enzymatic equilibrium fractionation (Mook et al., 1974). This is based on the observation that the rate-limiting step in the CA-mediated conversion of HCO_3^- to CO_2 is the actual dehydration of HCO_3^- to CO_2, instead of e.g. substrate binding (to Zn^{2+} within the enzyme) or product (CO_2) release, resulting in the observed CA-associated isotope fractionation to be very similar to the non-enzymatic fractionation (Paneth & O'Leary, 1985). Considering specifically this rate-limiting dehydration step is associated with a temperature dependent isotope effect (Mook et al., 1974), we implemented this into the model as such.

$$\frac{d(\delta^{13}C_{Cc})}{dt} = k_{f1}H_c(\delta^{13}C_{Hc} - \varepsilon_{HC}) - k_{r1}C_c(\delta^{13}C_{Cc} - \varepsilon_{CH}) + \frac{SA_{cyt}}{V_{cyt}}p_C(C_e\delta^{13}C_{Ce} - C_c\delta^{13}C_{Cc}) - \frac{SA_{ch}}{V_{cyt}}p_{ch}(C_c\delta^{13}C_{Cc} - C_{ch}\delta^{13}C_{Cch}) + 0.35 \cdot calc \cdot H_c \cdot (\delta^{13}C_{Hc} - \varepsilon_{calc}) \quad (15)$$

$$\frac{d(\delta^{13}C_{Cch})}{dt} = k_{f2}H_{ch}(\delta^{13}C_{Hch} - \varepsilon_{HC}) - k_{r2}C_{ch}(\delta^{13}C_{Cch} - \varepsilon_{CH}) + \frac{SA_{ch}}{V_{ch}}p_{ch}(C_c\delta^{13}C_{Cc} - C_{ch}\delta^{13}C_{Cch}) + \frac{SA_p}{V_{ch}}p_P(C_p\delta^{13}C_{Cp} - C_{ch}\delta^{13}C_{Cch}) \quad (16)$$

$$\frac{d(\delta^{13}C_{Hc})}{dt} = k_{r1}C_c(\delta^{13}C_{Cc} - \varepsilon_{CH}) - k_{f1}H_c(\delta^{13}C_{Hc} - \varepsilon_{HC}) - \frac{u_CH_c\delta^{13}C_{Hc}}{(K_n + H_c)}\frac{SA_{ch}}{V_{cyt}} + \frac{u_EH_e\delta^{13}C_{He}}{(K_n + H_e)}\frac{SA_{cyt}}{V_{cyt}} - 0.85 \cdot calc \cdot H_c \cdot (\delta^{13}C_{Hc} + \varepsilon_{calc}) \quad (17)$$

$$\frac{d(\delta^{13}C_{Hch})}{dt} = k_{r2}C_{ch}(\delta^{13}C_{Cch} - \varepsilon_{CH}) - k_{f2}H_{ch}(\delta^{13}C_{Hch} - \varepsilon_{HC}) + \frac{u_CH_c\delta^{13}C_{Hc}}{(K_n + H_c)}\frac{SA_{ch}}{V_{ch}} - \frac{u_{CH}H_{ch}\delta^{13}C_{Hch}}{(K_n + H_{ch})}\frac{SA_t}{V_{ch}} \quad (18)$$

https://doi.org/10.5194/egusphere-2026-3713
Preprint. Discussion started: 15 July 2026

$$\frac{d(\delta^{13}C_{Ct})}{dt} = k_{f3}H_t(\delta^{13}C_{Ht} - \varepsilon_{HC}) - k_{r3}C_t(\delta^{13}C_{Ct}\varepsilon_{CH}) + \frac{SA_p}{V_t}p_T\left(C_p\delta^{13}C_{Cp} - C_t\delta^{13}C_{Ct}\right) + \frac{SA_p}{V_t}p_T\left(C_p\delta^{13}C_{Cp} - C_t\delta^{13}C_{Ct}\right) \quad (19)$$

$$\frac{d(\delta^{13}C_{Ht})}{dt} = k_{r3}C_t(\delta^{13}C_{Ct} - \varepsilon_{CH}) - k_{f3}H_t(\delta^{13}C_{Ht} - \varepsilon_{HC}) + \frac{u_{CH}H_{ch}\delta^{13}C_{Hch}}{(K_n + H_{ch})}\frac{SA_t}{V_t} \quad (20)$$

$$\frac{d\left(\delta^{13}C_{Cp}\right)}{dt} = \frac{SA_p}{V_p}p_P\left(C_{ch}\delta^{13}C_{Cch} - C_p\delta^{13}C_{Cp}\right) + \frac{SA_p}{V_p}p_T\left(C_t\delta^{13}C_{Ct} - C_p\delta^{13}C_{Cp}\right) - r_1\left(\delta^{13}C_{Cp} - \varepsilon_{RuBP}\right) + k_{f4}H_p\left(\delta^{13}C_{Hp} - \varepsilon_{HC}\right) - k_{r4}C_p\left(\delta^{13}C_{Cp} - \varepsilon_{CH}\right) \quad (21)$$

$$\frac{d\left(\delta^{13}C_{Hp}\right)}{dt} = k_{r4}C_p\left(\delta^{13}C_{Cp} - \varepsilon_{CH}\right) - k_{f4}H_p\left(\delta^{13}C_{Hp} - \varepsilon_{HC}\right) \quad (22)$$

2.1.6 Determining ε_p

Rubisco fixes CO_2 into sugar in the pyrenoid, and therefore the $\delta^{13}C$ of the assimilated carbon ($\delta^{13}C_{sugar}$) is determined from $\delta^{13}C_{Cp} - \varepsilon_{Rubisco}$. Net stable carbon isotopic fractionation of the cell (ε_p) against the surrounding CO_2 pool (C_e) is then determined from $\delta^{13}C_{Ce} - \delta^{13}C_{sugar} + 2‰$. Here, the 2‰ represents a general $\delta^{13}C$ offset ($\varepsilon_{bulk\text{-}sugar}$) between bulk biomass and glucose in marine algae (Teece & Fogel, 2007).

2.2 Model behavior and culture fit

We investigated the general behavior of the model by simulating ε_p as a response to varying key parameters, notably temperature, the Michalis-Menten parameterization of HCO_3^- uptake, cell size, pyrenoid permeability, membrane permeability, calcification, carbon fixation rate, and $\varepsilon_{Rubisco}$.

Subsequently, three unconstrained parameters were used to fit modeled ε_p to measured ε_p of controlled growth experiments. Culture data of dinoflagellates (*Alexandrium tamarense*, *Gonyaulax spinifera*, *Protoceratium reticulatum* and *Scrippsiella trochoidea*) and *Gephyrocapsa huxleyi* (only calcifying diploid strains) were obtained from the literature (Bidigare et al., 1997; Hoins et al., 2015; Hoins, Eberlein, Groβmann, et al., 2016; Pearson et al., 2025; Riebesell et al., 2000; Rost et al., 2002; Wilkes et al., 2017) (Table 1). The tunable parameters represent the maximal enzymatic uptake rate of HCO_3^- (u_{max}), the uptake rate of HCO_3^- from the cytosol into the coccolith vesicle (referred to as the calcification rate, *calc*), and the pyrenoid permeability scaling factor (f_{pd}) (Table 1). All other parameters for the model are constrained based on empirical data and relations (Table 1 and A1). Optimal model-data fits are assessed using the root mean square error (RMSE) between simulations and observations.

https://doi.org/10.5194/egusphere-2026-3713
Preprint. Discussion started: 15 July 2026

Considering the value for the Michaelis parameter (K_n), for the specific dinoflagellate species used in this study the value is unconstrained, particularly for the individual compartments, which might have distinct Michaelis-Menten behavior and hence would need specific parameterizations. Therefore, for simplicity, K_n is set to 0 for dinoflagellates, which means there is a constant HCO_3^- uptake, equal to the maximal HCO_3^- uptake rate u_{max} (in mol s^{-1}). For *G. huxleyi*, K_n is set to $2 \cdot 10^{-7}$ mol cm^{-3} (200 µmol L^{-1}), which is the maximal value observed for *G. huxleyi* (Rost, Riebesell, et al., 2006) (see section 3.3 for a discussion on this value). Setting the K_n value to 200 µmol L^{-1} means that at a HCO_3^- concentration of 200 µmol L^{-1} the HCO_3^- uptake rate is half-maximal.

2.3 Validation of fitted model

To test the validity of the model fitted to culture data, *post hoc* model performance was evaluated by comparing simulations of three key processes with measurements from culture studies (Hoins, Eberlein, Van De Waal, et al., 2016b; Rost et al., 2002, 2003, 2006) that are not used as constrained parameters in the model. These processes are the relative HCO_3^- uptake (Eq. 23), CO_2 leakage (Eq. 24), and carbon isotope fractionation of particulate inorganic carbon (PIC) relative to CO_2 (ε_{PIC}) (Eq. 25 – 27).

Relative HCO_3^- uptake is determined according to the gross HCO_3^- uptake rate and total C_i uptake rate:

$$HCO_3^-: \text{total } C_i \text{ uptake} = \frac{\frac{u_{max} \cdot H_e}{K_n + H_e}}{p_c(C_e - C_c) + \frac{u_{max} \cdot H_e}{K_n + H_e}} \quad (23)$$

CO_2 leakage is calculated according to the CO_2 efflux (p_c x C_c) and influx (p_c x C_e) rate:

$$CO_2 \text{ leakage} = \frac{p_c(C_c)}{p_c(C_c) + p_c(C_e)} \quad (24)$$

ε_{PIC} is calculated as follows:

$$\varepsilon_{PIC} = \frac{\delta^{13}C_{Ce} - \delta^{13}C_{PIC}}{1 + \frac{\delta^{13}C_{PIC}}{1000}} \quad (25)$$

For this, $\delta^{13}C_{PIC}$ is determined using ODEs for PIC production and isotopic fluxes, with a carbon isotopic fractionation between HCO_3^- and PIC (ε_{calc}) of 1‰ (Zeebe & Wolf-Gladrow, 2001):

$$\frac{dPIC}{dt} = 0.85 \cdot calc \cdot H_c \quad (26)$$

$$\frac{d(\delta^{13}C_{PIC})}{dt} = 0.85 \cdot calc \cdot H_c \cdot (\delta^{13}C_{Hc} - \delta^{13}C_{PIC} + \varepsilon_{calc}) \quad (27)$$

https://doi.org/10.5194/egusphere-2026-3713
Preprint. Discussion started: 15 July 2026

All data analyses are done in R (R Core Team, 2023), using packages *seacarb* (Gattuso et al., 2023), *dplyr* (Wickham et al., 2014), *readxl* (Wickham and Bryan, 2015) and *ggplot2* (Wickham, 2016). For all parameters descriptions, see Table 1.

Table 1. Constrained and tunable parameters used in FRISO. Taxon-specific (i.e., dinoflagellate species and *G. huxleyi*) empirically constrained parameters and unconstrained tunable parameters are used to fit the model to culture data (see Table A1).

Parameter	Description
Constrained	
p_m	Membrane permeability (cm s^{-1}). Likely relates to temperature (Blanco-Ameijeiras et al., 2020).
pH_c	Cytosol pH
pH_{ch}	Chloroplast pH
pH_t	Thylakoid pH
pH_p	Pyrenoid pH
POC	Particulate organic carbon, organic carbon content of cultured cells (pg $cell^{-1}$)
V_{cell}	Cell volume (cm^3)
V_c	Cytosol volume (cm^3)
V_{ch}	Chloroplast volume (cm^3)
V_t	Thylakoid volume (cm^3)
V_p	Pyrenoid volume (cm^3)
SA_{cell}	Cell surface area (cm^2)
SA_c	Cytosol surface area (cm^2)
SA_{ch}	Chloroplast surface area (cm^2)
SA_t	Thylakoid surface area (cm^2)
SA_p	Pyrenoid surface area (cm^2)
$\varepsilon_{Rubisco}$	Rubisco associated stable carbon isotope fractionation (‰)
ε_{CH}	CA-mediated stable carbon isotope fractionation of CO_2 → HCO_3^- (‰)

https://doi.org/10.5194/egusphere-2026-3713
Preprint. Discussion started: 15 July 2026

ε_{HC}	CA-mediated stable carbon isotope fractionation of HCO_3^- → CO_2 (‰)
ε_{eq}	Non-enzymatic equilibrium fractionation of HCO_3^- ←→ CO_2 (‰)
ε_{calc}	Stable carbon isotope fractionation of HCO_3^- → $CaCO_3$
$\varepsilon_{bulk\text{-}sugar}$	$\delta^{13}C$ offset between bulk biomass and glucose in marine algae
$resp$	Respiratory carbon loss (%)
μ	Growth rate (s^{-1})
μ_i	Instantaneous growth rate (s^{-1})
r_1	Carbon fixation rate (mol cm^{-3} s^{-1})
K_m	Half-saturation (Michaelis) parameter of carbon fixation rate (mol cm^{-3})
K_1	Acid dissociation constant of HCO_3^- ←→ CO_2 (M)
k_{f1}	Forward reaction rate (HCO_3^- → CO_2) in cytosol (s^{-1})
k_{r1}	Reverse reaction rate (CO_2 → HCO3-) in cytosol (s^{-1})
k_{f2}	Forward reaction rate (HCO_3^- → CO2) in chloroplast (s^{-1})
k_{r2}	Reverse reaction rate (CO_2 → HCO_3^-) in chloroplast (s^{-1})
k_{f3}	Forward reaction rate (HCO_3^- → CO_2) in thylakoid (s^{-1})
k_{r3}	Reverse reaction rate (CO_2 → HCO_3^-) in thylakoid (s^{-1})
k_{f4}	Forward reaction rate (HCO_3^- → CO_2) in pyrenoid (s^{-1})
k_{r4}	Reverse reaction rate (CO_2 → HCO_3^-) in pyrenoid (s^{-1})
Tunable	
u_{max}	Maximal HCO_3^- uptake rate by membrane-bound transporters. Can depend on light intensity (PFD) (mol cm^{-2} s^{-1})
f_{pd}	Unitless scaling factor for the pyrenoid permeability (P_p). $P_p = f_{pd} \cdot p_m$. Depends on daylength.
$calc$	Calcification rate (s^{-1})

https://doi.org/10.5194/egusphere-2026-3713
Preprint. Discussion started: 15 July 2026

3 Results and discussion

3.1 General model behavior

The general behavior of the model was investigated under a range of parameter settings (Fig. 2). The findings of this are:

- Modeled ε_p increases with [$CO_{2\,(aq)}$] because it forces the influx of fresh CO_2, which reduces the accumulation of ^{13}C-enriched CO_2 in the cell.
- The carbon isotope fractionation of the modeled Rubisco enzyme ($\varepsilon_{Rubisco}$) fundamentally determines the upper limit of ε_p. However, the 2‰ $\delta^{13}C$ offset between bulk biomass and the sugar produced by photosynthesis ($\varepsilon_{bulk\text{-}sugar}$) (Sect. 2.1.6.) means maximum ε_p is higher than $\varepsilon_{Rubisco}$. Furthermore, calcification (*calc*) can force ε_p to even further exceed $\varepsilon_{Rubisco}$, as this removes relatively ^{13}C-enriched HCO_3^- from the cytosol, allowing accumulation of ^{12}C within the cell (Fig. 5).
- Increasing membrane permeability (p_m), and specifically the pyrenoid permeability (i.e., f_{pd}), causes higher ε_p, as it enhances inter-compartmental ventilation and higher influx of fresh CO_2 (Fig. 3).
- Modeled ε_p decreases with HCO_3^- uptake rate (u_{max}), as this enhances the uptake of relatively ^{13}C-enriched HCO_3^-.
- An increase in cell size (V_{cell}) forces a decrease in ε_p. This is because both CO_2 diffusion and HCO_3^- uptake are scaled to surface area and volume of the compartments (Eq. 3, 4). Bigger cell volumes result in lower surface area-to-volume ratios, which decreases CO_2 ventilation and thus reduces the influx of fresh CO_2 relative to the cell content (Fig. 3). However, the effect of V_{cell} on ε_p is small as compared to the other parameters.
- The Michaelis parameter of HCO_3^- uptake (K_n; the half-saturation HCO_3^- concentration) and temperature positively affect modeled ε_p in the lower range of [$CO_{2\,(aq)}$] (0 – 10 µM), but the overall effect is small compared to the other parameters. However, considering that culture experiments show temperature to force an increase in membrane permeability (in our model p_m), temperature likely substantially forces an increase in ε_p (Blanco-Ameijeiras et al., 2020).
- Lastly, higher fixation rates (r_f) force a decrease in ε_p as it increases carbon demand and ^{12}C-depletion (Fig. 3).

https://doi.org/10.5194/egusphere-2026-3713
Preprint. Discussion started: 15 July 2026

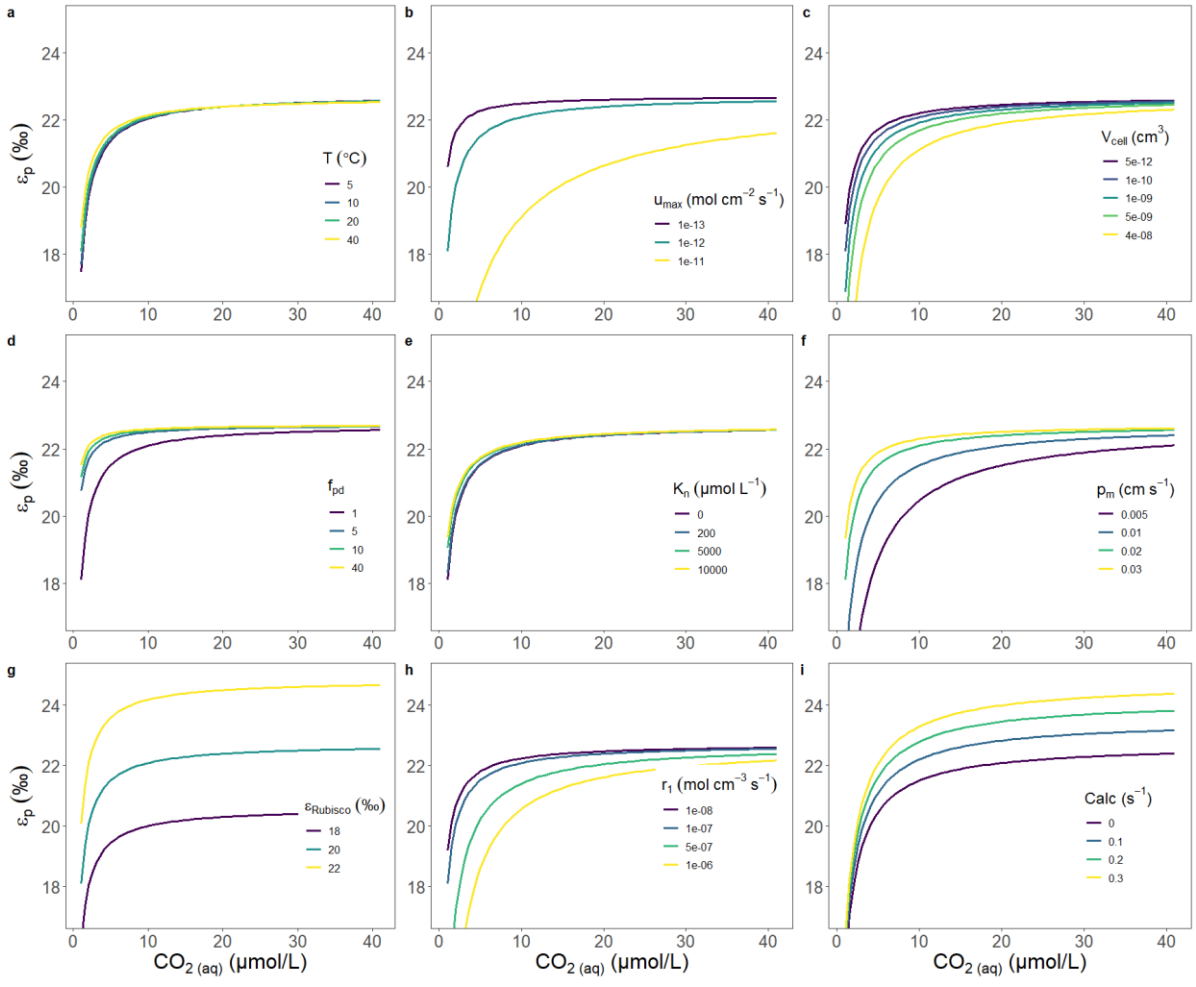

Figure 2: General model behavior. The effect of environmental and physiological factors on ε_p. (a) temperature (T), (b) maximal HCO_3^- uptake rate (u_{max}), (c) cell volume (V_{cell}), (d) pyrenoid permeability factor (f_{pd}), (e) Michaelis parameter of HCO_3^- uptake (K_n), (f) membrane permeability (p_m), (g) $\varepsilon_{Rubisco}$, (h) carbon fixation rate (r_1), and (i) calcification rate (calc). If not the varying parameter, the default settings are: $r_1 = 1x10^{-7}$ mol cm^{-3} s^{-1}, calc = 0 s^{-1}, $V_{cell} = 1x10^{-10}$ cm^3, T = 20 ℃, p_m = 0.02 cm s^{-1}, f_{pd} = 1 (unitless), $u_b = 1x10^{-12}$ mol cm^{-2} s^{-1}, $\varepsilon_{Rubisco}$ = 20‰.

https://doi.org/10.5194/egusphere-2026-3713
Preprint. Discussion started: 15 July 2026

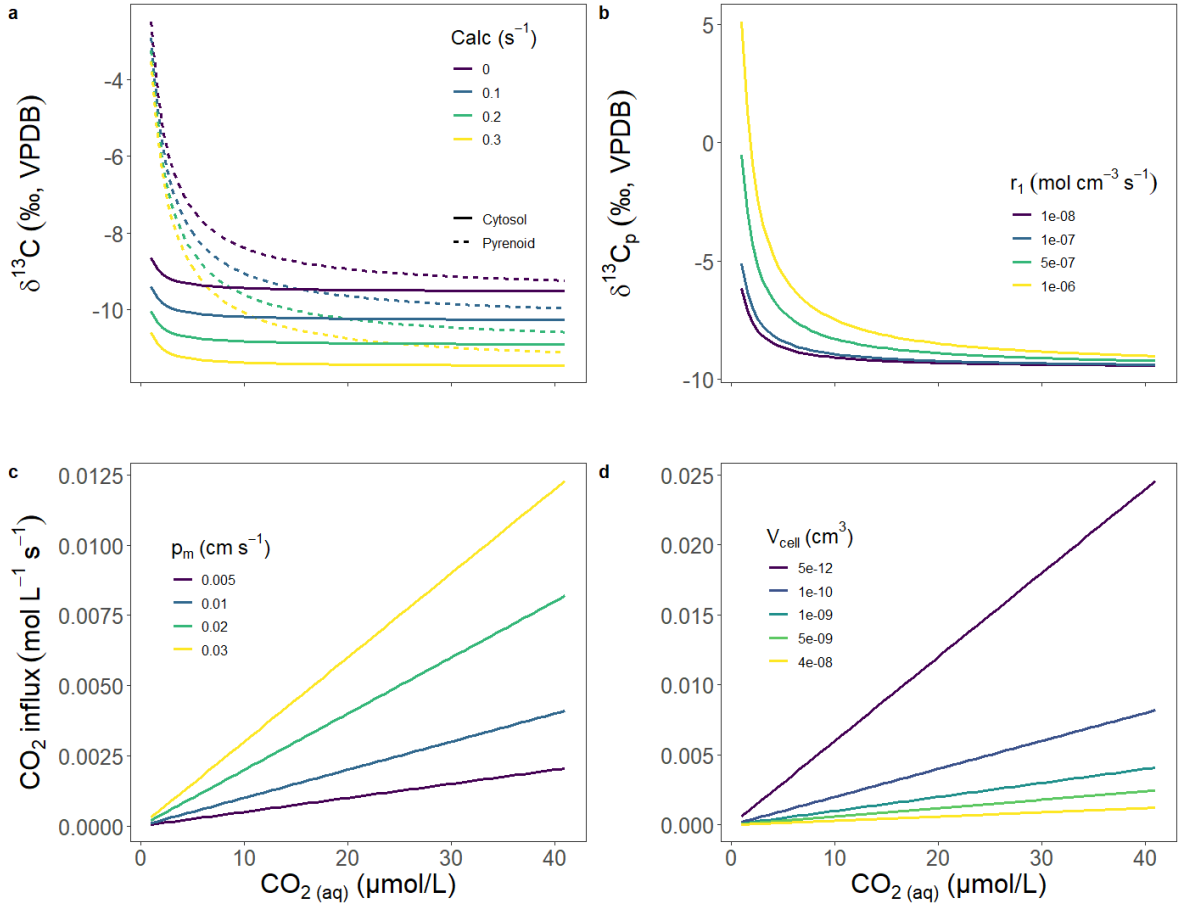

Figure 3: General model behavior (continued). a) The effect of calcification (*calc*) on $\delta^{13}C$ of CO_2 in the cytosol and pyrenoid, b) the effect of carbon fixation rate on $\delta^{13}C$ of CO_2 in the pyrenoid, c) the effect of membrane permeability (p_m) on CO_2 influx rate, and d) the effect of cell volume (V_{cell}) on CO_2 influx rate. If not the varying parameter, the default settings are: $r_1 = 1x10^{-7}$ mol cm^{-3} s^{-1}, calc = 0 s^{-1}, $V_{cell} = 1x10^{-10}$ cm^3, T = 20 ˚C, p_m = 0.02 cm s^{-1}, f_{pd} = 1 (unitless), $u_b = 1x10^{-12}$ mol cm^{-2} s^{-1}, $\varepsilon_{Rubisco}$ = 20‰. CO_2 influx rate = $p_m \cdot C_e \cdot SA_{cell}/V_{cell}$ (in mol L^{-1} s^{-1}).

3.2 Fitting model to culture data

To obtain the tunable model parameters u_{max}, f_{pd}, and *calc*, we fitted the model to culture data of dinoflagellates and *G. huxleyi* (Bidigare et al., 1997; Hoins et al., 2015; Hoins, Eberlein, Groβmann, et al., 2016; Pearson et al., 2025; Riebesell et al., 2000; Rost et al., 2002; Wilkes et al., 2017) (Fig. 4; see Table A1 for parameter values).

https://doi.org/10.5194/egusphere-2026-3713
Preprint. Discussion started: 15 July 2026

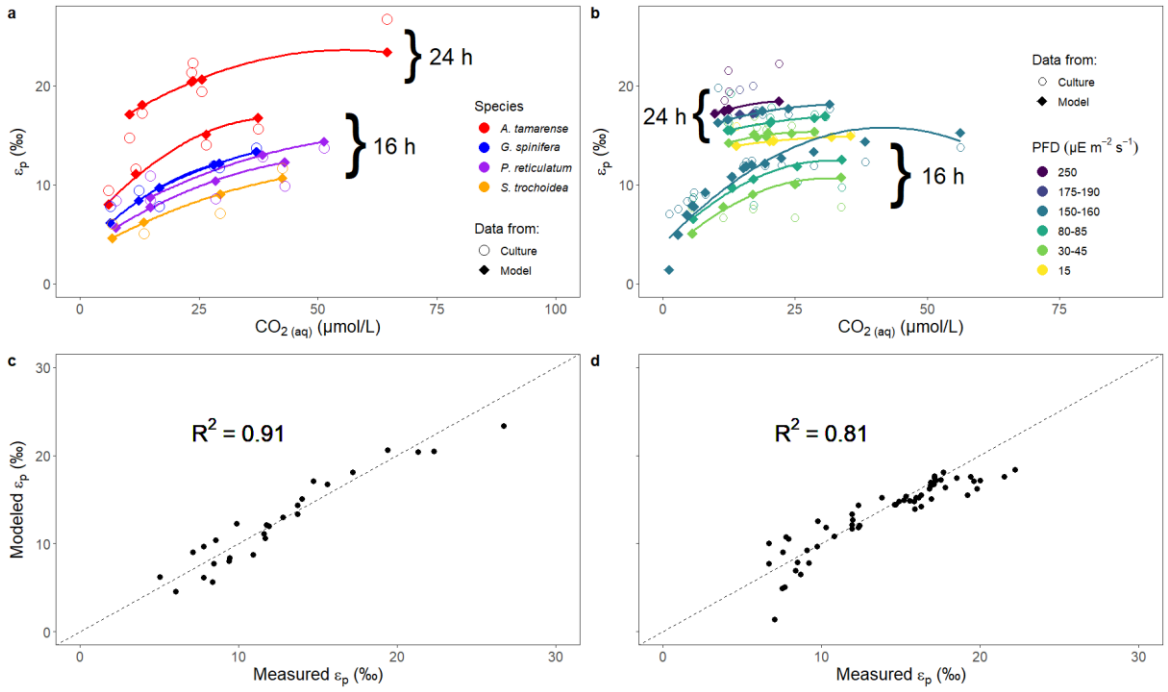

Figure 4: Model and culture data fit. Modeled (filled symbols and polynomial fit) versus corresponding culture (open symbols) ε_p values in dinoflagellates (Hoins et al., 2015; Hoins, Eberlein, Groβmann, et al., 2016; Wilkes et al., 2017) (a) and *G. huxleyi* (Bidigare et al., 1997; Pearson et al., 2025; Riebesell et al., 2000; Rost et al., 2002) (b) conducted under 16 and 24 h photoperiod conditions. In a) the colors represent the different dinoflagellate species, in b) the colors represent light intensity (PFD). In a) for *G. spinifera* and *P. reticulatum*, the two different lines represent culture experiments and model simulations run with a PFD of 250 and 55 µE m^{-2} s^{-1}. Panels c) and d) show correlations between culture and model results of a) and b), respectively. Dashed black lines are the 1:1 lines.

3.2.1 Dinoflagellate culture fit

For dinoflagellates, we used culture experiments with *Scrippsiella trochoidea*, *Alexandrium tamarense*, *Gonyaulax spinifera* and *Protoceratium reticulatum* (Hoins et al., 2015; Hoins, Eberlein, Groβmann, et al., 2016; Wilkes et al., 2017). The latter two were grown under low and high light conditions (photon flux density (PFD) of 55 and 250 µmol photons m^{-2} s^{-1}, respectively). This allows us to constrain the effect of light on HCO_3^- uptake (u_{max}) and ε_p, which should be light-dependent (Fig. 2). Accordingly, for *P. reticulatum*, u_{max} depends linearly on light intensity in our model (Eq. 4). As a result, ε_p decreases slightly with increasing light for this species (Fig. 4) – consistent with culture data (Hoins, Eberlein, Groβmann, et al., 2016). In contrast, *G. spinifera* ε_p seems to be insensitive to light, consistent with our model, for which the model-data fit is not improved with a light-dependent u_{max}.

The parameter f_{pd} (pyrenoid permeability) reflects changes in pyrenoid structure influenced by daylength, as reported in dinoflagellate literature (Nassoury et al., 2001). Therefore, f_{pd} depends on daylength in our model (Sect. 2.1.2), which makes the model consistent with ε_p values recorded in *A. tamarense* cultures exposed to both continuous light and a 16:8 h light/dark

https://doi.org/10.5194/egusphere-2026-3713
Preprint. Discussion started: 15 July 2026

cycle (Hoins et al., 2015; Wilkes et al., 2017). In total, the model explains 91% of the variance in ε_p across all cultured dinoflagellate data (R^2 = 0.91, RMSE = 1.56 ‰, Fig. 4c).

3.2.2 G. huxleyi culture fit

Since light-dependent uptake of HCO_3^- should lower ε_p, the positive correlation between ε_p and light found in *G. huxleyi* culture experiments (Pearson et al., 2025; Rost et al., 2002) may be surprising. However, this result illustrates that the effect of light on ε_p is primarily determined by light- and daylength-dependent calcification (Grubb et al., 2024; Nimer & Merrett, 1993), which increases ε_p by removing HCO_3^- (Fig. 2). Accordingly, we model the calcification rate to increase linearly with both PFD and daylength (Sect. 2.1.1.) – implying that daylength has a synergistic effect on calcification, in addition to PFD. Together with the daylength-dependent spatial configuration of the pyrenoid structure (i.e., f_{pd}) (cf. dinoflagellates), the model can fit the data of both 24 h and 16 h *G. huxleyi* culture experiments conducted under a range of PFD conditions. In total, the model explains 81% of the cultured *G. huxleyi* ε_p variance (R^2 = 0.81, RMSE = 1.88 ‰, Fig. 4d).

Intriguingly, the model accurately simulates observed ε_p values which are substantially higher than the $\varepsilon_{Rubisco}$ value of 11.1‰. This is due to the interplay of the implemented light-dependent calcification and daylength-dependent pyrenoid permeability, which allow for accumulation of ^{12}C in the cell, specifically in the pyrenoid, which results in an effective (observed) ε_p far exceeding the apparent maximum carbon isotope fractionation set by $\varepsilon_{Rubisco}$ (Fig. 5).

Evidently, the effect of light on ε_p of calcifying *G. huxleyi* is substantially larger than the effect of light on ε_p of non-calcifying dinoflagellates (Fig. 6).

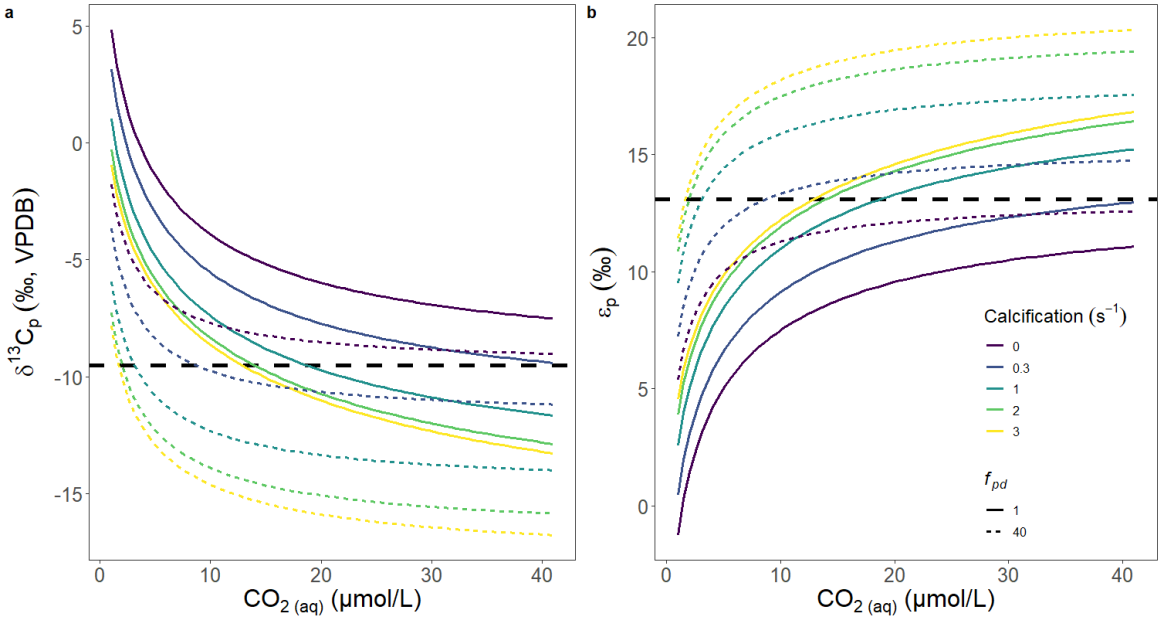

Figure 5: The effect of calcification and pyrenoid permeability (expressed using the pyrenoid permeability factor f_{pd} (Sect. 2.1.2)) on (a) $\delta^{13}C$ of the CO_2 in the pyrenoid ($\delta^{13}C_p$), and (b) ε_p, using *G. huxleyi* model settings. These

https://doi.org/10.5194/egusphere-2026-3713
Preprint. Discussion started: 15 July 2026

simulations use $\varepsilon_{Rubisco}$ = 11.1‰, u_{max} = 1.1e-11 mol cm^{-2} s^{-1}, p_m = 0.01 cm s^{-1}, V_{cell} = 1e-10 cm^3. The thick dashed horizontal line in (a) represents the $\delta^{13}C$ of the external (ambient) CO_2 pool ($\delta^{13}C_{Ce}$), which is the asymptote the simulated $\delta^{13}C_p$ approaches with increasing [$CO_{2\,(aq)}$] in the case of non-calcifying simulations (*calc* = 0). Similarly, in (b) the thick horizontal line represents the maximally possible ε_p value without calcification, which is determined by $\varepsilon_{Rubisco}$ + $\varepsilon_{bulk\text{-}sugar}$ (i.e., 11.1 + 2 = 13.1‰). Evidently, calcification allows for lowering $\delta^{13}C_p$ beyond $\delta^{13}C_{Ce}$, as calcification removes relatively ^{13}C-enriched HCO_3^- from the internal cellular environment. This allows for ε_p values exceeding 13.1‰. Note, f_{pd} of 1 and 40 correspond to daylengths of 16 and 24 hours respectively (Eq. 5).

3.3 *Post hoc* evaluation of model performance

The parameter settings as determined from the culture fit show that the environmental factors [$CO_{2\,(aq)}$] and light availability (PFD) have a substantial effect on modeled ε_p (Fig. 6) – a result consistent with surface sediment measurements associated with a wide range of natural light availability conditions (Phelps et al., 2021). Algal dimensions and physiological factors, including cell size and carbon fixation rate/growth rate, also affect modeled ε_p (Fig. 2). Culture studies in which all these parameters and processes are synergistically assessed are currently lacking. Therefore, *post hoc* model output is compared to various culture measurements, notably net cellular CO_2 leakage, relative HCO_3^- uptake, and ε_{PIC}, to evaluate if the model fit to culture results is forced by the correct underlying mechanisms. Lastly, we investigate the influence of total alkalinity (TA) on HCO_3^- uptake and ε_p values.

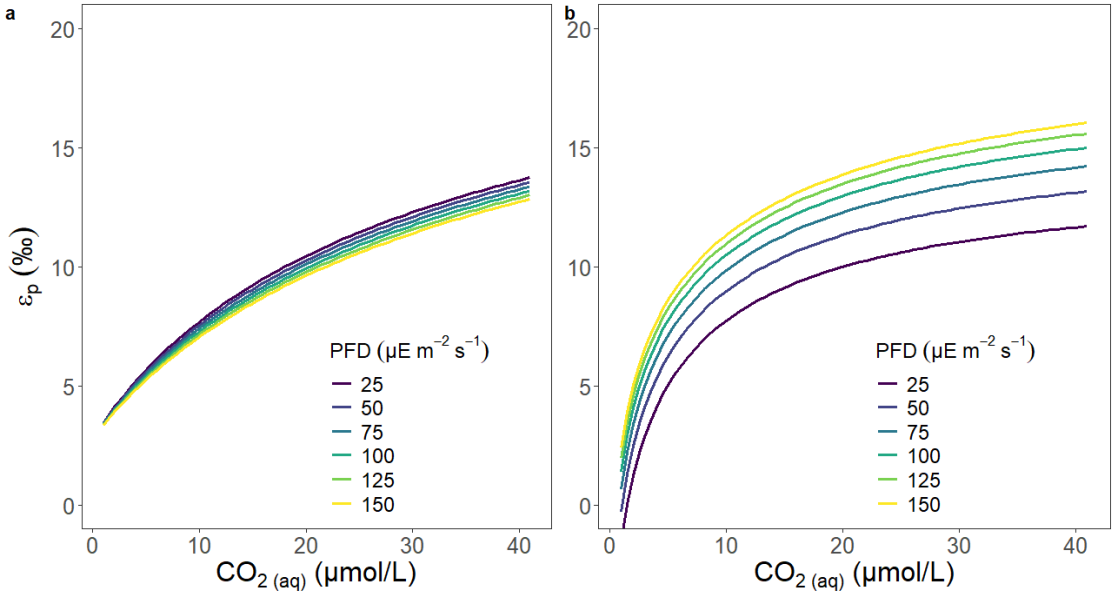

Figure 6: Model sensitivity to light availability (PFD) of dinoflagellate *P. reticulatum* (a) and *G. huxleyi* (b), using the parameter settings of the model fitted to respective culture data (Table A1). For *P. reticulatum* maximal HCO_3^- uptake rate (u_{max}) depends linearly on PFD (u_{max} = 9·10^{-13}·PFD + 5·10^{-10}). For *G. huxleyi*, u_{max} is constant (1.1·10^{-11} mol cm^{-2} s^{-1}), while calcification rate (*calc*) depends linearly on PFD and daylength (*calc* = 0.07·daylength + 0.01·PFD – 1.3). In this example, daylength is set to 16 h.

https://doi.org/10.5194/egusphere-2026-3713
Preprint. Discussion started: 15 July 2026

3.3.1 CO_2 leakage and relative HCO_3^- uptake

The model accurately simulates mean relative HCO_3^- uptake and CO_2 leakage for the dinoflagellates *A. tamarense*, *P. reticulatum* and *S. trochoidea*. However, relative HCO_3^- uptake is generally overestimated for *G. spinifera*. For *G. huxleyi*, the model accurately simulates mean CO_2 leakage and the $[CO_{2\,(aq)}]$-dependency of CO_2 leakage (Fig. 7). The model also correctly simulates the $[CO_{2\,(aq)}]$-dependency of relative HCO_3^- uptake (Fig. 7).

Nevertheless, although the model performs generally well, some discrepancies with experimental data emerge. Firstly, the model generally underestimates mean relative HCO_3^- uptake in *G. huxleyi* (Fig. 7). In dinoflagellates, the $[CO_{2\,(aq)}]$-dependency of the relative HCO_3^- uptake and leakage in the model (Fig. 7) is not observed in experiments (Hoins, Eberlein, Van De Waal, et al., 2016).

Such model-culture discrepancies could reflect issues with the modelling approach. However, it is argued (e.g. Badger et al., 1994; Hoins, Eberlein, Van De Waal, et al., 2016; Rost et al., 2003) that the membrane inlet mass spectrometry method used for assaying HCO_3^- uptake and cellular leakage in cultured algae (see Burkhardt et al. [2001] for a full description of the method) systematically underestimates leakage, as this is determined immediately after the light period when CO_2 is likely still being fixed. Furthermore, the method may well overestimate HCO_3^- uptake (Burkhardt et al., 2001). The HCO_3^- uptake assays are performed in a buffered medium with a constant pH of 8.0, possibly resulting in a higher HCO_3^- contribution than in the actual culturing conditions. Furthermore, assays are performed under PFD conditions of 300 µmol m^{-2} s^{-1}, which likely also results in higher apparent HCO_3^- uptake rates due the light-dependence of the associated membrane bound transporters. This could be the reason why there was not a consistent relationship observed between $[CO_{2\,(aq)}]$ and leakage/relative HCO_3^- uptake for dinoflagellates, even though this is suggested by our model results.

Alternatively, some of the underlying assumptions of our model could be inaccurate. For example, discrepancies between modeled and cultured relative HCO_3^- uptake and CO_2 leakage values might be due to other DIC transport processes within the algal cell, such as active CO_2 uptake (Rotatore et al., 1992), with or without CA-mediated conversion to HCO_3^- (cf. Wilkes and Pearson, 2019). Internal pumping of CO_2 allows for compartmental accumulation of CO_2, resulting in reduced passive diffusion from the environment into the cytosol (and thus higher relative HCO_3^- uptake). Furthermore, a ^{14}C isotopic disequilibrium study showed HCO_3^- uptake was $[CO_{2\,(aq)}]$-dependent, irrespective of light conditions (Kottmeier et al., 2014). Furthermore, genes associated with HCO_3^- transport are upregulated under low DIC conditions (Bach et al., 2013). This could suggest the Michaelis-Menten parameterization of HCO_3^- uptake in *G. huxleyi*, should also rely on $[CO_{2\,(aq)}]$. However, our simple approach, in which HCO_3^- uptake solely relies on $[HCO_3^-]$, accurately simulates the CO_2-dependency of HCO_3^- uptake (Fig. 7). This is because, per definition, relative HCO_3^- uptake increases when $[CO_{2\,(aq)}]$ decreases, as this reduces the passive influx of CO_2 into the cell, and thus increases the proportion of active HCO_3^- uptake.

https://doi.org/10.5194/egusphere-2026-3713
Preprint. Discussion started: 15 July 2026

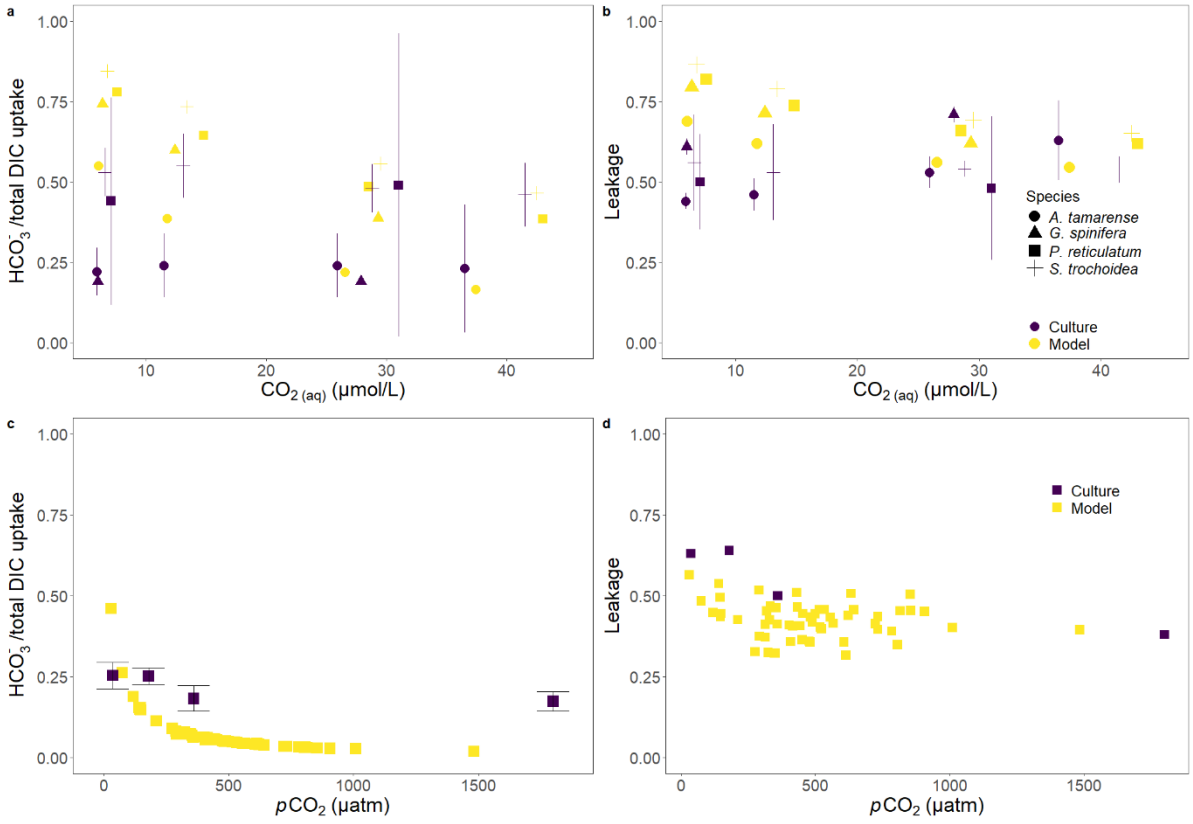

Figure 7: Modeled relative HCO_3^- uptake and CO_2 leakage. (a) and (b) for dinoflagellates under a 16 h photoperiod compared to culture measurements of Hoins et al. (2016). (c) and (d) for *G. huxleyi* compared to culture measurements of Rost et al. (2003; 2006). Plots (c) and (d) are plotted as a function of pCO_2 because [$CO_{2\,(aq)}$] data was lacking (Rost et al., 2003; 2006). Error bars represent 95% CI of culture measurements.

3.3.2 Simulated ε_{PIC} values in *G. huxleyi*

325 The model generally simulates ε_{PIC} values in line with culture measurements (Fig. 8). A *t*-test comparing modeled and measured ε_{PIC} values shows no significant difference ($t(65) = -1.56$, $p > 0.05$). However, in our model simulations, ε_{PIC} increases with light intensity (Fig. 8) whereas the culture study of Rost et al. (2002) shows a decrease. This likely relates to our simplified implementation of calcification, which assumes direct uptake of HCO_3^- and precipitation of $CaCO_3$ in the cytosol. In reality, the coccolith vesicle is a highly controlled environment in which ion fluxes are precisely regulated for
330 $CaCO_3$ crystallization (e.g., Kadan et al., 2021; McClelland et al., 2017). Considering the scope of our model is to accurately simulate the mechanisms behind organic – and not inorganic – carbon isotope fractionation, our relatively simple incorporation of calcification, which on average simulates ε_{PIC} values in line with culture data, suffices for this application.

https://doi.org/10.5194/egusphere-2026-3713
Preprint. Discussion started: 15 July 2026

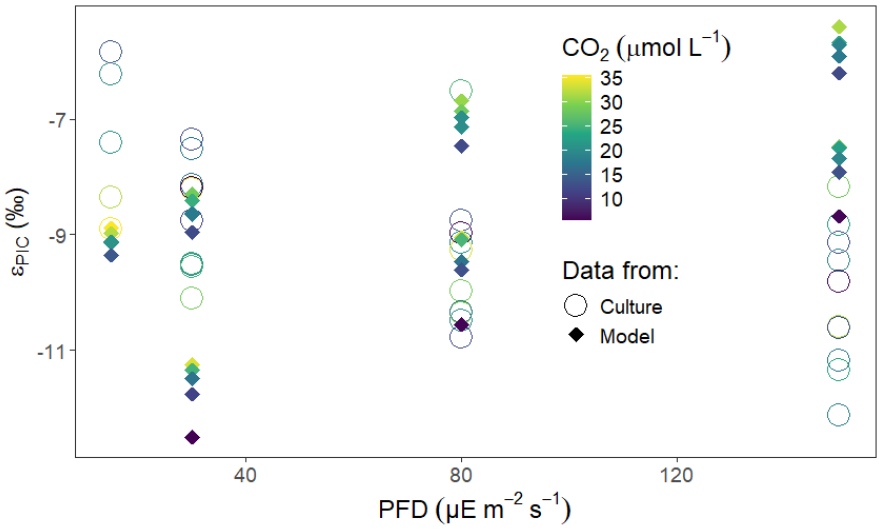

Figure 8: Simulated ε_{PIC} values as compared to culture measurements from Rost et al. (2002), as a function of PFD and [CO_2 (aq)].

3.3.3 The influence of alkalinity and the haploid stage

For dinoflagellates, we assumed a constant HCO_3^- uptake rate, by setting the Michaelis constant (K_n) to zero, even though for certain dinoflagellate species (i.e., *Protocentrum minimum* and *Heterocapsa triquetra*) HCO_3^- uptake depends on [$HCO_{3\,(aq)}^-$] (Rost, Richter, et al., 2006). Yet, for the dinoflagellate species used in this model the value of K_n is unconstrained. Importantly, setting K_n to 400 µM – as found maximally for dinoflagellates and *G. huxleyi* (Rost, Richter, et al., 2006) – does not affect the model fit (R^2 = 0.9, RMSE = 1.6 ‰). Also, the model response of relative uptake of HCO_3^- to changes in total alkalinity (TA) is not substantially affected by K_n. This results in ε_p to be rather insensitive to changes in TA – and thus [$HCO_{3\,(aq)}^-$] – when K_n is set to 400 µM (Fig. 9).

https://doi.org/10.5194/egusphere-2026-3713
Preprint. Discussion started: 15 July 2026

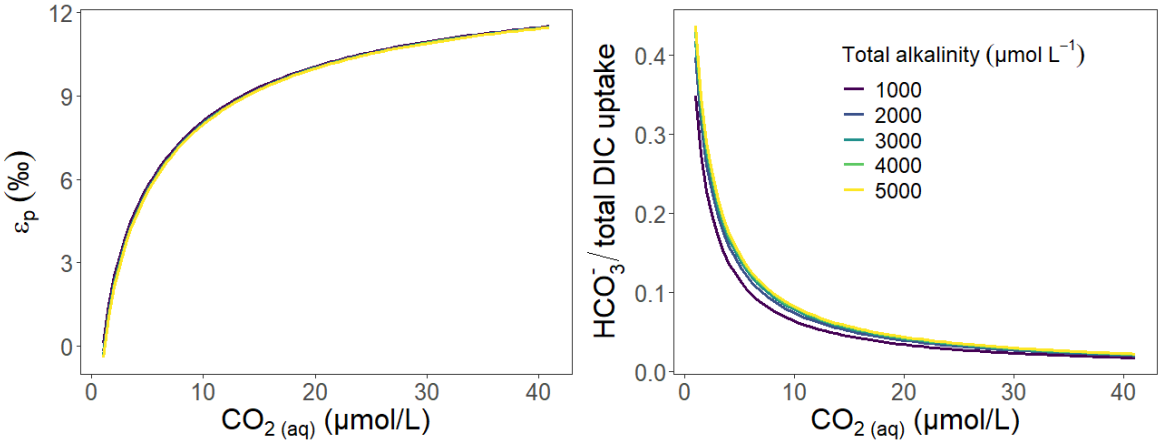

Figure 9: Model response to total alkalinity (TA). These simulations use *G. huxleyi* model parameter settings, ($\varepsilon_{Rubisco}$ = 11.1‰, u_{max} = 1.1e-11 mol cm^{-2} s^{-1}, p_m = 0.01 cm s^{-1}, V_{cell} = 1e-10 cm^3) and K_n = 400 µM.

Lastly, Bidigare et al. (1997) found similar ε_p values between the diploid calcifying and haploid non-calcifying *G. huxleyi*, which suggests no effect of calcification on ε_p, using a chemostat culturing setup with a constant washout rate. However, this method has been criticized for producing ε_p values that may not reflect natural conditions, as the dilution rate may be too high to allow the DIC pool in the culture medium to reach isotopic equilibrium (Zhang et al., 2022). Therefore, their result may be affected by these disequilibrium conditions. In our model, calcification substantially impacts ε_p (Fig. 2), and we argue that calcification should affect ε_p as it draws from the cytosolic HCO_3^- pool, thereby affecting internal carbonate chemistry of the alga, and also the $\delta^{13}C$ of the internal DIC pool. The latter is reflected in calcification rate-dependent $\delta^{13}C_{calcite}$ values of cultured *G. huxleyi* (Grubb et al., 2024). Future controlled batch cultures on calcifying and non-calcifying *G. huxleyi* strains might provide additional constraints on the influence of calcification on carbon isotope fractionation.

3.4 Considerations for future research

Overall, our results demonstrate that the model of ^{13}C-fractionation based on diffusion of CO_2 and active HCO_3^- transport (Sharkey & Berry, 1985), modulated by environmental and physiological factors, accurately explains experimental data from cultured dinoflagellates and *G. huxleyi*. The mechanistic model explains a dominant part of the variability in culture experiments by simulating the impact of carbonate chemistry and light availability on the resulting inorganic carbon fluxes. It is positively evaluated by correspondence with culture-constrained physiological properties that emerge from the model. Importantly, the model can realistically simulate ε_p values exceeding $\varepsilon_{Rubisco}$, by means of compartmentalized accumulation of ^{12}C.

Our approach does not require statistical corrections (Stoll et al., 2019) or hypothetical enzymes that induce fractionation (Wilkes and Pearson, 2019). Instead, it describes light and carbonate system-dependent processes evident from culture studies.

https://doi.org/10.5194/egusphere-2026-3713
Preprint. Discussion started: 15 July 2026

That is, passive influx of CO_2, the diurnal forcing of the pyrenoid structure (Nassoury et al., 2001), and light-dependent active transport of HCO_3^- (Nakajima et al., 2013; Omata et al., 1999) and calcification (Grubb et al., 2024; Nimer & Merrett, 1993).

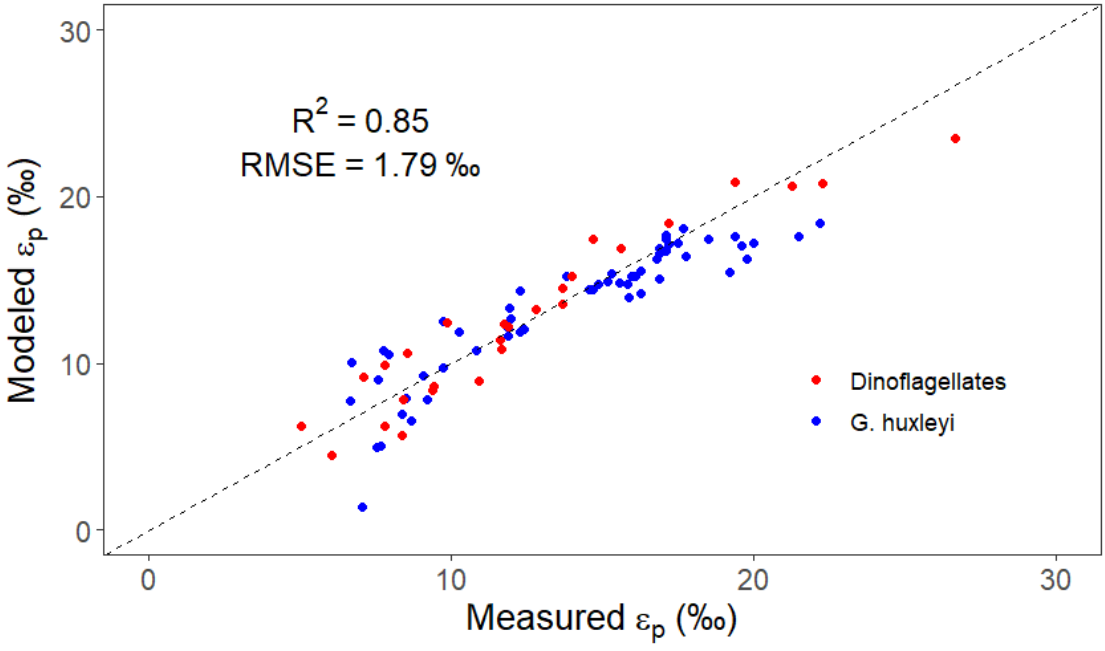

Figure 10: Total model fit. Correlation between culture and modeled ε_p. Dashed black lines is the 1:1 line.

Our fitted model can potentially be used for reconstructions of past CO_2 concentrations, based on sedimentary measurements of fossilized dinoflagellate cysts and *Gephyrocapsa*-derived alkenones (Frieling et al., 2023; Phelps et al., 2021). For this, all other parameters that force ε_p must be constrained. These are cell size, carbon fixation rate, temperature, daylength, and light availability (PFD).

Firstly, the size of dinoflagellate cysts directly relates to the size of the dinoflagellate that produced them (Finkel et al., 2007). For alkenones, size measurements of fossil coccoliths can be used to determine the size of the alkenone-producer (Hendriks & Pagani, 2007). Secondly, considering open ocean conditions generally result in algal growth rates far below laboratory conditions (Phelps et al., 2021), it is reasonable to assume carbon fixation rates (r_l in our model) are generally always below $1 \cdot 10^{-7}$ mol cm^{-3} s^{-1}, which is above the maximum value found for culture studies. This implies carbon fixation rates will have a negligible effect on ε_p (Fig. 2). Thirdly, temperature can be constrained using conventional seawater temperature proxies, as has been practice for this line of proxies for decades. Fourthly, daylength can be estimated based on (paleo-)latitude. Finally, light availability (PFD) remains extremely difficult to constrain, although some avenues could be explored based on thermocline- and habitat-depth reconstructions (e.g., Spero et al., 2003). Alternatively, a large range of possible PFD values can be used as input in the model to evaluate uncertainty. A subsequent bootstrapping approach (cf. Wubben et al., 2026) can give $[CO_{2\,(aq)}]$ reconstructions with intrinsic uncertainties.

https://doi.org/10.5194/egusphere-2026-3713
Preprint. Discussion started: 15 July 2026

Lastly, although in our model temperature has only a small effect on ε_p, we might expect the effect of temperature to be larger. Culture experiments have shown that membrane permeability is significantly affected by temperature (Blanco-Ameijeiras et al., 2020). Since membrane permeability (p_m in our model) has a substantial influence on ε_p, this should affect ε_p accordingly. Culture studies have not explored this effect in detail; the cited culture studies have used temperatures between 15 and 18 °C. However, sedimentary studies of both dinoflagellate cysts and alkenones, and marine particulate organic matter in general (Frieling et al., 2023; Liu et al. 2022; Phelps et al., 2021), indeed show a significant relationship between ε_p and temperature. Therefore, when using this model for the investigation of surface sediment measurements or reconstructions, a temperature-dependent membrane permeability (p_m), for example based on measurements of Blanco-Ameijeiras et al. (2020), should be taken into account.

4 Conclusion

Our model (FRISO) of ^{13}C-fractionation in algae, based on CO_2 diffusion and active HCO_3^- uptake, accurately simulates inorganic carbon fluxes and ε_p in algal cells during controlled growth experiments of multiple species, including coccolithophores and dinoflagellates. The model shows that, in addition to external [$CO_{2\,(aq)}$], the influence of light on HCO_3^- transport is an important driver of ε_p. Therefore, we advise future culturing studies to put extra emphasis on studying the effects of light on cellular HCO_3^- uptake and calcification. This could improve mechanistic models such as FRISO, and hence reconstructions of past pCO_2.

Appendix A

Table A1. Parameter settings of the model fit to culture data of dinoflagellates (*A. tamarense*, *S. trochoidea*, *G. spinifera* and *P. reticulatum*) and *G. huxleyi*.

Parameter	Dinoflagellates	*G. huxleyi*	Reference/notes
Taxon specific			
p_m	0.027	0.01	Hopkinson et al. (2011), Wilkes & Pearson (2019), Blanco-Ameijeiras et al. (2020)
pH_c	7	7	Cf. Wilkes & Pearson (2019)
pH_{ch}	8	8	Cf. Wilkes & Pearson (2019)
pH_t	6	6	Cf. Wilkes & Pearson (2019)

https://doi.org/10.5194/egusphere-2026-3713
Preprint. Discussion started: 15 July 2026

pH_p	8	8	Cf. Wilkes & Pearson (2019)
V_{cell}	$1.24 \cdot POC^{1.22} \cdot 10^{-12}$	$3.51 \cdot POC^{1.14} \cdot 10^{-12}$	Menden-Deuer and Lessard (2000); Popp et al. (1998)
V_c	$0.847 \cdot V_{cell}$	$0.847 \cdot V_{cell}$	Wilkes and Pearson (2019)
V_{ch}	$0.09 \cdot V_{cell}$	$0.09 \cdot V_{cell}$	Hopkinson et al. (2011), van de Meene et al. (2012), Wilkes & Pearson (2019)
V_t	$0.06 \cdot V_{cell}$	$0.06 \cdot V_{cell}$	Hopkinson et al. (2011), van de Meene et al. (2012); Wilkes & Pearson (2019)
V_p	$0.003 \cdot V_{cell}$	$0.003 \cdot V_{cell}$	Hopkinson et al. (2011), van de Meene et al. (2012), Wilkes & Pearson (2019)
SA_{cell}	Derived from V_{cell}	Derived from V_{cell}	Assuming spherical shape
SA_c	Derived from V_c	Derived from V_c	Assuming spherical shape
SA_{ch}	Derived from V_{ch}	Derived from V_{ch}	Assuming spherical shape
SA_t	Derived from V_t	Derived from V_t	Assuming spherical shape
SA_p	Derived from V_p	Derived from V_p	Assuming spherical shape
$\varepsilon_{Rubisco}$	24	11.1	Guy (1993), McNevin et al. (2007), Robinson et al. (2003), Boller et al. (2011)
ε_{HC}	$9.866 \cdot \frac{1000}{T + 273.15} - 24.12$	$9.866 \cdot \frac{1000}{T + 273.15} - 24.12$	Mook et al. (1974), Paneth & O'Leary, (1985). T in ˚C
ε_{CH}	0	0	
ε_{eq}	$9.866 \cdot \frac{1000}{T + 273.15} - 24.12$	$9.866 \cdot \frac{1000}{T + 273.15} - 24.12$	Mook et al. (1974), Paneth & O'Leary (1985). T in ˚C
ε_{calc}	1	1	Zeebe & Wolf-Gladrow (2001)
$\varepsilon_{bulk\text{-}sugar}$	2	2	Teece & Fogel (2007)
$resp$	15%	15%	Rost et al. (2002), Laws and Bannister (1980)
μ_i	$\frac{\mu \cdot (L + D)}{L - D \cdot resp}$	$\frac{\mu \cdot (L + D)}{L - D \cdot resp}$	Rost et al. (2002), Laws and Bannister (1980). L and D are durations of light (L) and dark (D) period.

https://doi.org/10.5194/egusphere-2026-3713
Preprint. Discussion started: 15 July 2026

r_1	POC · μ_i	POC · μ_i	
K_1	First dissociation constant of carbonic acid	First dissociation constant of carbonic acid	*seacarb* in R, Gattuso et al., 2023
k_{f1}	$\frac{10^{-pH_c}}{K_1} \cdot 10^6$	$\frac{10^{-pH_c}}{K_1} \cdot 10^6$	Assumed to occur quasi-instantaneously (i.e. multiplied by 10^6)
k_{r1}	$\frac{K_1}{10^{-pH_c}} \cdot 10^6$	$\frac{K_1}{10^{-pH_c}} \cdot 10^6$	Assumed to occur quasi-instantaneously (i.e. multiplied by 10^6)
k_{f2}	$\frac{10^{-pH_{ch}}}{K_1} \cdot 10^6$	$\frac{10^{-pH_{ch}}}{K_1} \cdot 10^6$	Assumed to occur quasi-instantaneously (i.e. multiplied by 10^6)
k_{r2}	$\frac{K_1}{10^{-pH_{ch}}} \cdot 10^6$	$\frac{K_1}{10^{-pH_{ch}}} \cdot 10^6$	Assumed to occur quasi-instantaneously (i.e. multiplied by 10^6)
k_{f3}	$\frac{10^{-pH_t}}{K_1} \cdot 10^6$	$\frac{10^{-pH_t}}{K_1} \cdot 10^6$	Assumed to occur quasi-instantaneously (i.e. multiplied by 10^6)
k_{r3}	$\frac{K_1}{10^{-pH_t}} \cdot 10^6$	$\frac{K_1}{10^{-pH_t}} \cdot 10^6$	Assumed to occur quasi-instantaneously (i.e. multiplied by 10^6)
k_{f4}	$\frac{10^{-pH_p}}{K_1} \cdot 10^6$	$\frac{10^{-pH_p}}{K_1} \cdot 10^6$	Assumed to occur quasi-instantaneously (i.e. multiplied by 10^6)
k_{r4}	$\frac{K_1}{10^{-pH_p}} \cdot 10^6$	$\frac{K_1}{10^{-pH_p}} \cdot 10^6$	Assumed to occur quasi-instantaneously (i.e. multiplied by 10^6)
Tunable			
u_{max}	$2\text{x}10^{-10}$ for *A. tamarense* $5\text{x}10^{-10}$ for *S. trochoidea* $1\text{x}10^{-9}$ for *G. spinifera* $9\text{x}10^{-13} + 5\text{x}10^{-10} \cdot$ PFD for *P. reticulatum*	$1.1\text{x}10^{-11}$	Relationship with PFD only found for *P. reticulatum* (Hoins et al., 2016)
f_{pd}	$= \begin{cases} 10, & \text{if daylength} = 24 \\ 1, & \text{otherwise} \end{cases}$	$= \begin{cases} 40, & \text{if daylength} = 24 \\ 1, & \text{otherwise} \end{cases}$	f_{pd} scaled to daylength, only for photoperiod range used in culture studies
p_p	$p_m \cdot f_{pd}$	$p_m \cdot f_{pd}$	Scaling of the regular membrane permeability p_m
calc	0	0.07 · daylight + 0.007 · PFD – 1.3	Linearly scaled to daylength and PFD

https://doi.org/10.5194/egusphere-2026-3713
Preprint. Discussion started: 15 July 2026

Code and data availability

The R scripts, underlying research data, and user manual for the model are publicly available (under the MIT license) and have been deposited in a Zenodo repository at https://doi.org/10.5281/ZENODO.20812734 (Bats et al., 2026). This repository is permanently archived and linked to the active development version maintained on GitHub at https://github.com/yfbats/FRISO-Physiological-model-for-algal-13C-fractionation.

Author contributions

YFB: Conceptualization, Data curation, Formal analysis, Investigation, Methodology, Software, Validation, Visualization, Writing – original draft. **AS:** Conceptualization, Funding acquisition, Project administration, Supervision, Validation, Writing – review & editing. **GJR:** Conceptualization, Funding acquisition, Project administration, Supervision, Validation, Writing – review & editing.

Competing interests

The authors declare there are no competing interests.

Disclaimer

Copernicus Publications remains neutral with regard to jurisdictional claims made in the text, published maps, institutional affiliations, or any other geographical representation in this paper. While Copernicus Publications makes every effort to include appropriate place names, the final responsibility lies with the authors. Views expressed in the text are those of the authors and do not necessarily reflect the views of the publisher.

Acknowledgements

YFB thanks the organizers of the alkenone CO_2 pre-conference workshop (Goldschmidt 2025, Prague) for covering travel costs to their inspiring workshop, which resulted in fruitful discussions on the alkenone CO_2 proxy.

https://doi.org/10.5194/egusphere-2026-3713
Preprint. Discussion started: 15 July 2026

Financial support

This work was funded by an award of the Ammodo Foundation to AS, for unfettered research. This work was also supported by EMBRACER (Summit grant no. SUMMIT.1.034), financed by the Netherlands Organization for Scientific Research (NWO).

References

Bach, L. T., Mackinder, L. C. M., Schulz, K. G., Wheeler, G., Schroeder, D. C., Brownlee, C., & Riebesell, U. (2013). Dissecting the impact of CO2 and PH on the mechanisms of photosynthesis and calcification in the coccolithophore Gephyrocapsa huxleyi. New Phytologist, 199(1), 121–134. https://doi.org/10.1111/nph.12225

Badger, M. P. S., Chalk, T. B., Foster, G. L., Bown, P. R., Gibbs, S. J., Sexton, P. F., Schmidt, D. N., Pälike, H., Mackensen, A., & Pancost, R. D. (2019). Insensitivity of alkenone carbon isotopes to atmospheric CO2 at low to moderate CO2 levels. Climate of the Past, 15(2), 539–554. https://doi.org/10.5194/cp-15-539-2019

Badger, M. R., Palmqvist, K., & Yu, J. (1994). Measurement of CO2 and HCO3− fluxes in cyanobacteria and microalgae during steady-state photosynthesis. Physiologia Plantarum, 90(3), 529–536. https://doi.org/10.1111/j.1399-3054.1994.tb08811.x

Barber, J., Mills, J., & Nicolson, J. (1974). Studies with cation specific ionophores show that within the intact chloroplast Mg++ acts as the main exchange cation for H+ pumping. FEBS Letters, 49(1), 106–110. https://doi.org/10.1016/0014-5793(74)80643-5

Bats, Y.F. (2026). FRISO (v1.0): Physiological model for algal 13C-fractionation (Version v1.0) [Computer software]. Zenodo. https://doi.org/10.5281/ZENODO.20812734

Bidigare, R. R., Fluegge, A., Freeman, K. H., Hanson, K. L., Hayes, J. M., Hollander, D., Jasper, J. P., King, L. L., Laws, E. A., Milder, J., Millero, F. J., Pancost, R., Popp, B. N., Steinberg, P. A., & Wakeham, S. G. (1997). Consistent fractionation of13 C in nature and in the laboratory: Growth-rate effects in some haptophyte algae. Global Biogeochemical Cycles, 11(2), 279–292. https://doi.org/10.1029/96GB03939

Blanco-Ameijeiras, S., Stoll, H. M., Zhang, H., & Hopkinson, B. M. (2020). Influence of temperature and CO2 on plasma-membrane permeability to CO2 and HCO3− in the marine haptophytes Emiliania huxleyi and Calcidiscus leptoporus (Prymnesiophyceae). Journal of phycology, 56(5), 1283-1294.

https://doi.org/10.5194/egusphere-2026-3713
Preprint. Discussion started: 15 July 2026

Boller, A. J., Thomas, P. J., Cavanaugh, C. M., & Scott, K. M. (2011). Low stable carbon isotope fractionation by coccolithophore RubisCO. Geochimica et Cosmochimica Acta, 75(22), 7200–7207. https://doi.org/10.1016/j.gca.2011.08.031

Brandenburg, K. M., Rost, B., Van de Waal, D. B., Hoins, M., & Sluijs, A. (2022). Physiological control on carbon isotope fractionation in marine phytoplankton. Biogeosciences, 19(13), 3305–3315. https://doi.org/10.5194/bg-19-3305-2022

Burkhardt, S., Amoroso, G., Riebesell, U., & Sültemeyer, D. (2001). CO2 and HCO3− uptake in marine diatoms acclimated to different CO2 concentrations. Limnology and Oceanography, 46(6), 1378–1391. https://doi.org/10.4319/lo.2001.46.6.1378

Burns, B. D., & Beardall, J. (1987). Utilization of inorganic carbon by marine microalgae. Journal of Experimental Marine Biology and Ecology, 107(1), 75–86. https://doi.org/10.1016/0022-0981(87)90125-0

Cassar, N., Laws, E. A., & Popp, B. N. (2006). Carbon isotopic fractionation by the marine diatom Phaeodactylum tricornutum under nutrient- and light-limited growth conditions. Geochimica et Cosmochimica Acta, 70(21), 5323–5335. https://doi.org/10.1016/j.gca.2006.08.024

Checchetto, V., Segalla, A., Allorent, G., La Rocca, N., Leanza, L., Giacometti, G. M., Uozumi, N., Finazzi, G., Bergantino, E., & Szabò, I. (2012). Thylakoid potassium channel is required for efficient photosynthesis in cyanobacteria. Proceedings of the National Academy of Sciences, 109(27), 11043–11048. https://doi.org/10.1073/pnas.1205960109

Checchetto, V., Teardo, E., Carraretto, L., Formentin, E., Bergantino, E., Giacometti, G. M., & Szabo, I. (2013). Regulation of photosynthesis by ion channels in cyanobacteria and higher plants. Biophysical Chemistry, 182, 51–57. https://doi.org/10.1016/j.bpc.2013.06.006

Cohen, W. S., & Jagendorf, A. T. (1974). Further Studies on the Bicarbonate Stimulation of Photophosphorylation in Isolated Chloroplastsl. 53.

De Boer, R. (2024, June 25). Grind.R. https://tbb.bio.uu.nl/rdb/grindR/

E. & Wolf, L. M. (2025). Isolating the light dependence of carbon isotope fractionation in

Farquhar, G., O'Leary, M., & Berry, J. (1982). On the Relationship Between Carbon Isotope Discrimination and the Intercellular Carbon Dioxide Concentration in Leaves. Functional Plant Biology, 9(2), 121. https://doi.org/10.1071/PP9820121

Finkel, Z. V., Sebbo, J., Feist-Burkhardt, S., Irwin, A. J., Katz, M. E., Schofield, O. M. E., Young, J. R., & Falkowski, P. G. (2007). A universal driver of macroevolutionary change in the size of marine phytoplankton over the Cenozoic. Proceedings of the National Academy of Sciences, 104(51), 20416–20420. https://doi.org/10.1073/pnas.0709381104

https://doi.org/10.5194/egusphere-2026-3713
Preprint. Discussion started: 15 July 2026

Francois, R., Altabet, M. A., Goericke, R., McCorkle, D. C., Brunet, C., & Poisson, A. (1993). Changes in the δ13 C of surface water particulate organic matter across the subtropical convergence in the SW Indian Ocean. Global Biogeochemical Cycles, 7(3), 627–644. https://doi.org/10.1029/93GB01277

Freeman, K. H., & Hayes, J. M. (1992). Fractionation of carbon isotopes by phytoplankton and estimates of ancient CO 2 levels. Global Biogeochemical Cycles, 6(2), 185–198. https://doi.org/10.1029/92GB00190

Frieling, J., Van Roij, L., Kleij, I., Reichart, G.-J., & Sluijs, A. (2023). Single-species dinoflagellate cyst carbon isotope fractionation in core-top sediments: Environmental controls, CO 2 dependency and proxy potential. Biogeosciences, 20(22), 4651–4668. https://doi.org/10.5194/bg-20-4651-2023

Gattuso, J.-P., Epitalon, J.-M., Lavigne, H., Orr, J., Gentili, B., Hagens, M., Hofmann, A., Mueller, J.-D., Proye, A., Rae, J., & Soetaert, K. (2023). seacarb: Seawater Carbonate Chemistry. R package version 3.3.2. https://CRAN.R-project.org/package=seacarb

Grubb, A. R., Johns, C. T., Hayden, M. G., Subhas, A. V., Thamatrakoln, K., & Bidle, K. D. (2024). Calcification increases carbon supply, photosynthesis, and growth in a globally distributed coccolithophore. Limnology and Oceanography, 69(9), 2152–2166. https://doi.org/10.1002/lno.12656

Guy, R. D. (1993). Photosynthetic Fractionation of the Stable lsotopes of Oxygen and Carbon'. 101.

Henderiks, J., & Pagani, M. (2007). Refining ancient carbon dioxide estimates: Significance of coccolithophore cell size for alkenone-based pCO2 records. Paleoceanography, 22(3). https://doi.org/10.1029/2006pa001399

Hoins, M., Eberlein, T., Groβmann, C. H., Brandenburg, K., Reichart, G.-J., Rost, B., Sluijs, A., & Van de Waal, D. B. (2016). Combined Effects of Ocean Acidification and Light or Nitrogen Availabilities on 13C Fractionation in Marine Dinoflagellates. PLOS ONE, 11(5), e0154370. https://doi.org/10.1371/journal.pone.0154370

Hoins, M., Eberlein, T., Van De Waal, D. B., Sluijs, A., Reichart, G.-J., & Rost, B. (2016). CO2-dependent carbon isotope fractionation in dinoflagellates relates to their inorganic carbon fluxes. Journal of Experimental Marine Biology and Ecology, 481, 9–14. https://doi.org/10.1016/j.jembe.2016.04.001

Hoins, M., Van De Waal, D. B., Eberlein, T., Reichart, G.-J., Rost, B., & Sluijs, A. (2015). Stable carbon isotope fractionation of organic cyst-forming dinoflagellates: Evaluating the potential for a CO2 proxy. Geochimica et Cosmochimica Acta, 160, 267–276. https://doi.org/10.1016/j.gca.2015.04.001

Hoins, M., Van De Waal, D. B., Eberlein, T., Reichart, G.-J., Rost, B., & Sluijs, A. (2015). Stable carbon isotope fractionation of organic cyst-forming dinoflagellates: Evaluating the potential for a CO2 proxy. Geochimica et Cosmochimica Acta, 160, 267–276. https://doi.org/10.1016/j.gca.2015.04.001

https://doi.org/10.5194/egusphere-2026-3713
Preprint. Discussion started: 15 July 2026

Holtz, L.-M., Wolf-Gladrow, D., & Thoms, S. (2015). Simulating the effects of light intensity and carbonate system composition on particulate organic and inorganic carbon production in Emiliania huxleyi. Journal of Theoretical Biology, 372, 192–204. https://doi.org/10.1016/j.jtbi.2015.02.024

Holtz, L.-M., Thoms, S., & Wolf-Gladrow, D. A. (2017). Stable carbon isotope signals in particulate organic and inorganic carbon of coccolithophores – A numerical model study for Emiliania huxleyi. Journal of Theoretical Biology, 420, 117–127. https://doi.org/10.1016/j.jtbi.2017.01.030

Hopkinson, B. M., Dupont, C. L., Allen, A. E., & Morel, F. M. M. (2011). Efficiency of the CO2-concentrating mechanism of diatoms. https://doi.org/10.1016/j.gca.2025.09.033

Intergovernmental Panel on Climate Change (IPCC). (2023). Climate Change 2021 – The Physical Science Basis. Cambridge University Press. https://doi.org/10.1017/9781009157896

Kadan, Y., Tollervey, F., Varsano, N., Mahamid, J., & Gal, A. (2021). Intracellular nanoscale architecture as a master regulator of calcium carbonate crystallization in marine microalgae. Proceedings of the National Academy of Sciences, 118(46). https://doi.org/10.1073/pnas.2025670118

Kottmeier, D. M., Rokitta, S. D., Tortell, P. D., & Rost, B. (2014). Strong shift from HCO3 − to CO2 uptake in Gephyrocapsa huxleyi with acidification: New approach unravels acclimation versus short-term pH effects. Photosynthesis Research, 121(2–3), 265–275. https://doi.org/10.1007/s11120-014-9984-9

Laws, E. A., & Bannister, T. T. (1980). Nutrient- and light-limited growth of Thalassiosira fluviatilis in continuous culture, with implications for phytoplankton growth in the ocean1. Limnology and Oceanography, 25(3), 457–473. https://doi.org/10.4319/lo.1980.25.3.0457

Laws, E. A., Bidigare, R. R., & Popp, B. N. (1997). Effect of growth rate and CO2 concentration on carbon isotopic fractionation by the marine diatom Phaeodactylum tricornutum. Limnology and Oceanography, 42(7), 1552–1560. https://doi.org/10.4319/lo.1997.42.7.1552

Liu, Q., Kandasamy, S., Zhai, W., Wang, H., Veeran, Y., Gao, A., & Chen, C.-T. A. (2022). Temperature is a better predictor of stable carbon isotopic compositions in marine particulates than dissolved CO2 concentration. Communications Earth & Environment, 3(1). https://doi.org/10.1038/s43247-022-00627-y

McClelland, H. L. O., Bruggeman, J., Hermoso, M., & Rickaby, R. E. M. (2017). The origin of carbon isotope vital effects in coccolith calcite. Nature Communications, 8(1), 14511. https://doi.org/10.1038/ncomms14511

McNevin, D. B., Badger, M. R., Whitney, S. M., von Caemmerer, S., Tcherkez, G. G. B., & Farquhar, G. D. (2007). Differences in Carbon Isotope Discrimination of Three Variants of D-Ribulose-1,5-bisphosphate Carboxylase/Oxygenase

https://doi.org/10.5194/egusphere-2026-3713
Preprint. Discussion started: 15 July 2026

Reflect Differences in Their Catalytic Mechanisms. Journal of Biological Chemistry, 282(49), 36068–36076. https://doi.org/10.1074/jbc.M706274200

Meer, M. & Sluijs, A. (2025). Evidence for limited atmospheric CO2 rise at the onset of the Miocene Climatic Optimum. ESS Open Archive. https://doi.org/10.22541/essoar.175881368.82469378/v1

Menden-Deuer, S., & Lessard, E. J. (2000). Carbon to volume relationships for dinoflagellates, diatoms, and other protist plankton. Limnology and Oceanography, 45(3), 569–579. https://doi.org/10.4319/lo.2000.45.3.0569

Middelburg, J. J. (2019). Biogeochemical Processes and Inorganic Carbon Dynamics. In SpringerBriefs in Earth System Sciences (pp. 77–105). Springer International Publishing. https://doi.org/10.1007/978-3-030-10822-9_5

Moisan, T. A., Ellisman, M. H., Buitenhuys, C. W., & Sosinsky, G. E. (2006). Differences in chloroplast ultrastructure of Phaeocystis antarctica in low and high light. Marine Biology, 149(6), 1281–1290. https://doi.org/10.1007/s00227-006-0321-5

Moisan, T. A., Ellisman, M. H., Buitenhuys, C. W., & Sosinsky, G. E. (2006). Differences in chloroplast ultrastructure of Phaeocystis antarctica in low and high light. Marine Biology, 149(6), 1281–1290. https://doi.org/10.1007/s00227-006-0321-5

Mook, W. G., Bommerson, J. C., & Staverman, W. H. (1974). Carbon isotope fractionation between dissolved bicarbonate and gaseous carbon dioxide. Earth and Planetary Science Letters, 22(2), 169–176. https://doi.org/10.1016/0012-821X(74)90078-8

Nakajima, K., Tanaka, A., & Matsuda, Y. (2013). SLC4 family transporters in a marine diatom directly pump bicarbonate from seawater. Proceedings of the National Academy of Sciences, 110(5), 1767–1772. https://doi.org/10.1073/pnas.1216234110

Nassoury, N., Fritz, L., & Morse, D. (2001). Circadian Changes in Ribulose-1,5-Bisphosphate Carboxylase/Oxygenase Distribution Inside Individual Chloroplasts Can Account for the Rhythm in Dinoflagellate Carbon Fixation.

Nimer, N. A., & Merrett, M. J. (1993). Calcification rate in Emiliania huxleyi Lohmann in response to light, nitrate and availability of inorganic carbon. New Phytologist, 123(4), 673–677. https://doi.org/10.1111/j.1469-8137.1993.tb03776.x

Omata, T., Price, G. D., Badger, M. R., Okamura, M., Gohta, S., & Ogawa, T. (1999). Identification of an ATP-binding cassette transporter involved in bicarbonate uptake in the cyanobacterium Synechococcus sp. Strain PCC 7942. Proceedings of the National Academy of Sciences, 96(23), 13571–13576. https://doi.org/10.1073/pnas.96.23.13571

Paneth, P., & O'Leary, M. H. (1985). Carbon isotope effect on dehydration of bicarbonate ion catalyzed by carbonic anhydrase. Biochemistry, 24(19), 5143–5147. https://doi.org/10.1021/bi00340a028

https://doi.org/10.5194/egusphere-2026-3713
Preprint. Discussion started: 15 July 2026

Pearson, A., Polissar, P. J., Carter, S. J., Kocharian, E., Phelps, S. R., Hover, O. D., Reis, R.P., Kuang, Phelps, S. R., Stoll, H. M., Bolton, C. T., Beaufort, L., & Polissar, P. J. (2021). Controls on Alkenone Carbon Isotope Fractionation in the Modern Ocean. Geochemistry, Geophysics, Geosystems, 22(12), e2021GC009658. https://doi.org/10.1029/2021GC009658

Popp, B. N., Kenig, F., Wakeham, S. G., Laws, E. A., & Bidigare, R. R. (1998). Does growth rate affect ketone unsaturation and intracellular carbon isotopic variability in Emiliania huxleyi ? Paleoceanography, 13(1), 35–41. https://doi.org/10.1029/97PA02594

Popp, B. N., Laws, E. A., Bidigare, R. R., Dore, J. E., Hanson, K. L., & Wakeham, S. G. (1998). Effect of Phytoplankton Cell Geometry on Carbon Isotopic Fractionation. Geochimica et Cosmochimica Acta, 62(1), 69–77. https://doi.org/10.1016/S0016-7037(97)00333-5

Pottosin, I. I., & Schönknecht, G. (1995). Patch clamp study of the voltage-dependent anion channel in the thylakoid membrane. The Journal of Membrane Biology, 148(2). https://doi.org/10.1007/BF00207270

R Core Team (2023). _R: A Language and Environment for Statistical Computing_. R Foundation for Statistical Computing, Vienna, Austria. <https://www.R-project.org/>.

Riebesell, U., Revill, A. T., Holdsworth, D. G., & Volkman, J. K. (2000). The effects of varying CO2 concentration on lipid composition and carbon isotope fractionation in Gephyrocapsa huxleyi. Geochimica et Cosmochimica Acta, 64(24), 4179–4192. https://doi.org/10.1016/S0016-7037(00)00474-9

Robinson, J. J., Scott, K. M., Swanson, S. T., O'Leary, M. H., Horken, K., Tabita, F. R., & Cavanaugh, C. M. (2003). Kinetic isotope effect and characterization of form II RubisCO from the chemoautotrophic endosymbionts of the hydrothermal vent tubeworm Riftia pachyptila. Limnology and Oceanography, 48(1), 48–54. https://doi.org/10.4319/lo.2003.48.1.0048

Rost, B., Richter, K., Riebesell, U., & Hansen, P. J. (2006). Inorganic carbon acquisition in red tide dinoflagellates. Plant, Cell & Environment, 29(5), 810–822. https://doi.org/10.1111/j.1365-3040.2005.01450.x

Rost, B., Riebesell, U., & Burkhardt, S. (2003). Carbon acquisition of bloom-forming marine phytoplankton. Limnology and Oceanography, 48(1), 55–67.

Rost, B., Riebesell, U., & Sültemeyer, D. (2006). Carbon acquisition of marine phytoplankton: Effect of photoperiod length. Limnology and Oceanography, 51(1), 12–20. https://doi.org/10.4319/lo.2006.51.1.0012

Rost, B., Zondervan, I., & Riebesell, U. (2002). Light-dependent carbon isotope fractionation in the coccolithophorid Gephyrocapsa huxleyi. Limnology and Oceanography, 47(1), 120–128.

https://doi.org/10.5194/egusphere-2026-3713
Preprint. Discussion started: 15 July 2026

Rotatore, C., Lew, RogerR., & Colman, B. (1992). Active uptake of CO2 during photosynthesis in the green alga Eremosphaera viridis is mediated by a CO2-ATPase. Planta, 188(4). https://doi.org/10.1007/BF00197046

Sharkey, T. D., & Berry, J. A. (1985). CARBON ISOTOPE FRACTIONATION OF ALGAE AS INFLUENCED BY AN INDUCIBLE CO2 CONCENTRATING MECHANISM.

Spero, H. J., Mielke, K. M., Kalve, E. M., Lea, D. W., & Pak, D. K. (2003). Multispecies approach to reconstructing eastern equatorial Pacific thermocline hydrography during the past 360 kyr. Paleoceanography, 18(1). https://doi.org/10.1029/2002pa000814

Stoll, H. M., Guitian, J., Hernandez-Almeida, I., Mejia, L. M., Phelps, S., Polissar, P., Rosenthal, Y., Zhang, H., & Ziveri, P. (2019). Upregulation of phytoplankton carbon concentrating mechanisms during low CO2 glacial periods and implications for the phytoplankton pCO2 proxy. Quaternary Science Reviews, 208, 1–20. https://doi.org/10.1016/j.quascirev.2019.01.012

Teece, M. A., & Fogel, M. L. (2007). Stable carbon isotope biogeochemistry of monosaccharides in aquatic organisms and terrestrial plants. Organic Geochemistry, 38(3), 458–473. https://doi.org/10.1016/j.orggeochem.2006.06.008

Tester, M., & Blatt, M. R. (1989). Direct Measurement of K+ Channels in Thylakoid Membranes by Incorporation of Vesicles into Planar Lipid Bilayers. Plant Physiology, 91(1), 249–252. https://doi.org/10.1104/pp.91.1.249

van de Meene, A. M. L., Sharp, W. P., McDaniel, J. H., Friedrich, H., Vermaas, W. F. J., & Roberson, R. W. (2012). Gross morphological changes in thylakoid membrane structure are associated with photosystem I deletion in Synechocystis sp. PCC 6803. Biochimica et Biophysica Acta (BBA) - Biomembranes, 1818(5), 1427–1434. https://doi.org/10.1016/j.bbamem.2012.01.019

Vidyarathna, N. K., Smith, L. E., Miller, K. R., Coyne, K. J., Cohen, J. H., & Warner, M. E. (2024). Short-term and long-term exposure to combined elevated temperature and CO2 leads to differential growth, toxicity, and fatty acid profiles in the harmful dinoflagellate Karlodinium veneficum. Frontiers in Marine Science, 11, 1305495. https://doi.org/10.3389/fmars.2024.1305495

Wang, Z., Tong, S., Xu, D., Huang, X., Sun, Y., Wang, B., Sun, H., Zhang, X., Fan, X., Wang, W., Sun, K., Wang, Y., Zhang, P., Gu, Z., & Ye, N. (2024). Effects of temperature and nitrogen sources on physiological performance of the coccolithophore Emiliania huxleyi. Marine Environmental Research, 196, 106405. https://doi.org/10.1016/j.marenvres.2024.106405

Wickham, H. (with Sievert, C.). (2016). ggplot2: Elegant graphics for data analysis (Second edition). Springer international publishing.

https://doi.org/10.5194/egusphere-2026-3713
Preprint. Discussion started: 15 July 2026

Wickham, H., & Bryan, J. (2015). readxl: Read Excel Files [Dataset]. In CRAN: Contributed Packages. The R Foundation. https://doi.org/10.32614/cran.package.readxl

Wickham, H., François, R., Henry, L., Müllr, K., & Vaughan, D. (2014). dplyr: A Grammar of Data Manipulation [Dataset]. In CRAN: Contributed Packages. The R Foundation. https://doi.org/10.32614/cran.package.dplyr

Wijker, R. S., Aguiló-Nicolau, P., Jaggi, M., Galmés, J., & Stoll, H. M. (2026). A simplified approach for measuring Rubisco carbon isotope fractionation and the first determination in marine haptophyte Gephyrocapsa oceanica. Biogeosciences, 23(4), 1591–1608. https://doi.org/10.5194/bg-23-1591-2026

Wilkes, E. B., & Pearson, A. (2019). A general model for carbon isotopes in red-lineage phytoplankton: Interplay between unidirectional processes and fractionation by RubisCO. Geochimica et Cosmochimica Acta, 265, 163–181. https://doi.org/10.1016/j.gca.2019.08.043

Wilkes, E. B., Carter, S. J., & Pearson, A. (2017). CO2-dependent carbon isotope fractionation in the dinoflagellate Alexandrium tamarense. Geochimica et Cosmochimica Acta, 212, 48–61. https://doi.org/10.1016/j.gca.2017.05.037

Wubben, E., Frieling, J., Bats, Y. F., van Roij, L., de Haan, K., Reichart, G., Peterse, F., Sangiorgi, F., van der Meer, M. T. J., & Sluijs, A. (2026). Evidence for Limited Atmospheric CO2 Rise at the Miocene Climatic Optimum. Paleoceanography and Paleoclimatology, 41(6). https://doi.org/10.1029/2025pa005388

Zeebe, R. E., & Wolf-Gladrow, D. (2001). CO2 in seawater: Equilibrium, kinetics, isotopes (Vol. 65).

Zhang, Y., & Gao, K. (2021). Photosynthesis and calcification of the coccolithophore Gephyrocapsa huxleyi are more sensitive to changed levels of light and CO2 under nutrient limitation. Journal of Photochemistry and Photobiology B: Biology, 217, 112145. https://doi.org/10.1016/j.jphotobiol.2021.112145

Zhang, H., Torres-Romero, I., Anjewierden, P., Jaggi, M., & Stoll, H. M. (2022). The DIC carbon isotope evolutions during CO2 bubbling: Implications for ocean acidification laboratory culture. Frontiers in Marine Science, 9. https://doi.org/10.3389/fmars.2022.1045634

Zolotareva, E. K., Polishchuk, O. V., Semenikhin, A. V., & Onoiko, E. B. (2013). The Contribution of Light-Dependent Bicarbonate Uptake in Thylakoid Membrane Energization. In Advanced Topics in Science and Technology in China (pp. 197–201). Springer Berlin Heidelberg. https://doi.org/10.1007/978-3-642-32034-7_41